공학박사학위논문

Safe Design for Hydrogen Production and Transportation Systems

수소 생산 및 수송시스템의 안전한 디자인 및 관리 설계

2020 년 8 월

서울대학교 대학원

화학생물공학부 에너지환경 화학융합기술

이 건 학

Abstract

Safe Design for Hydrogen Production and Transportation Systems

Gunhak Lee
School of Chemical & Biological Engineering
The Graduate School
Seoul National University

International demand for hydrogen is increasing. In particular, after the spread of electric vehicles, hydrogen has been connected not only with chemical plants, but also with people's living life. In this paper, the safe design of a hydrogen refueling station for electronic vehicle and the prediction of the corrosion damage of a pipe defect for the safe management of a hydrogen underground buried pipe is studied.

First, the safe design of a hydrogen refueling station targets a process that produces hydrogen from natural gas-derived material, which is known to be the most economical. This is a comparison of three processes: the first is to load hydrogen produced from the outside of the station carried by a high-pressure trailer, and then transform its pressure to meet the demand. The second is to produce hydrogen from gaseous NG(natural gas) through steam reforming reaction, and the last is the process of producing hydrogen by steam reforming reaction through LPG.

All three processes is found to exceed tolerable risk levels in areas with some population density under currently known process conditions. Therefore, it is possible to safely design the process by changing the conditions of the process units that most affect the risk to mitigate the risk, or lower the frequency of failure event occurring by constructing additional firewalls.

On the other hand, off-site pipelines placed to transport the produced hydrogen going out of the hydrogen station or the incoming hydrogen from the outside are mainly installed in a buried form. Buried piping is an inevitable structure for the utilization of the ground area, but it is difficult to check the condition frequently due to the limitations of drilling costs and human resources to directly check the condition of the piping. Therefore, more attention should be paid to safety management. In particular, buried piping accidents in areas close to the population, such as Kaohsiung in Taiwan or San Bruno in the United States, can cause personal injury, so evaluate and predict whether the risk or reliability of piping is safe and secure in the future. It is important to do.

There have been many studies predicting the defect depth distribution of pipes due to external corrosion. Predictive modeling of the previous papers were well predicted defect depths measured in the soil environments. However, the external corrosion of piping is affected by

various environmental factors, so a well-made model may be inaccurate in other environments. This is because a large amount of data is required and it is generally difficult to apply to changing soils. To overcome this, the Adaptive Bayesian methodology is needed.

Predicting Defect Depth well can be said to have established a model for how quickly the defect depth is growing. Defect Depth Growth rate model, that is, prediction model for External Corrosion rate, has also been studied. Like Defect Depth, since it is affected by various environmental variables, the Adaptive model is effective for general prediction.

Therefore, through this, it was possible to study a more accurate prediction model of the defect depth for the safe design of the hydrogen filling station and the reliability measurement of the pipe that transports hydrogen to the outside of the filling station. It is a demand for a more careful and safe design for the hydrogen charging

station in the vicinity of a person, and it is expected that through the above study, a safe hydrogen storage will be installed and managed.

Keywords: Hydrogen, Quantitative Risk Assessment, Reliability ; Monte-carlo simulation ; Limit state function ; failure mode ; underground pipeline

Student Number: 2014-21591

Abstract in Korean (국문초록)

수소에 대한 국제 수요가 점차 증가하고 있다. 특히 전기자동차의 보급 이후, 수소는 화학플랜트에서 뿐만 아니라, 도시에서 있는 사람들의 생활권과도 맞닿아 있다. 이 논문에서는 전기자동차에 수소를 공급받기 위한 수소충전소의 안전한 설계와 해당 수소충전소의 외부로, 혹은 외부에서 수소가 이송될 경우 이용하게 될 수소 지하매설배관의 안전한 관리를 위한 배관결함의 손상도 예측을 연구하였다.

먼저 수소충전소에 대한 안전한 설계는 수소를 가장 경제적으로 생산할 수 있다고 알려진 천연가스로부터 생산하는 공정을 대상으로 한다. 이는 3 가지 공정을 비교할 수 있는데, 첫번째는 외부에서 생산된 수소를 고압 트레일러로 싣고 온 후, 수요에 맞게 변압하는 공정이고, 두번째는 기체상태의 NG 에서 수소를 Steam Reforming Reaction 으로 생산하는 공정, 마지막으로 LPG 에서 수소를 Steam Reforming 하여 생산하는 공정이다.

세 공정 모두 현재 알려진 공정 조건에서는 인구밀도가 어느 정도 있는 지역에서 모두 Tolerable 한 위험도 수준을 넘어서는 것으로 나타났다. 따라서 위험도에 가장 많이 영향을 주는 공정

유닛들의 조건들을 조금씩 바꿔가며 위험도를 낮추는 공정 수정을 하여 안전한 공정설계를 할 수 있다.

한편, 수소충전소 외부로 나가는 생산된 수소, 혹은 외부에서 들어오는 수소를 이송하기 위해 놓여지는 Off-site 파이프라인들은 주로 매설된 형태로 설치가 된다. 매설배관은 지상면적의 활용을 위해 필연적인 구조물이지만, 배관 상태를 직접 확인하기 위한 굴착비용 및 인적 자원의 한계 등으로 자주 상태를 확인하기 힘들다. 따라서 안전관리에 더욱 유의하여야 한다. 특히 대만의 가오슝(Kaohsiung)이나 미국의 산 브루노(San Bruno) 사고처럼 인구 밀접 지역에서의 매설배관사고는 인명피해를 유발할 수 있어, 현재 및 향후에 배관의 위험도나 신뢰도가 안전한 수준인지 평가하고 예측하는 것이 중요하다.

외부부식에 따른 배관의 Defect Depth 분포를 예측하는 연구들이 많이 있어왔다. 선행 논문들의 예측 모델링들은 해당 토양환경들에서 직접 측정한 Defect Depth 들을 잘 예측한 모델들이었다. 하지만 배관의 외부부식은 여러가지의 환경요소에 영향을 받고, 따라서 잘 만들어진 모델도 다른 환경에서는 부정확할 수 있다. 대량의 데이터가 필요하고, 변화하는 토양에 일반적으로 적용하기 힘들기 때문이다. 이를 극복하기 위해 Adaptive Bayesian 방법론이 필요하다.

Defect Depth 를 잘 예측한다는 것은 defect depth 가 얼마나 빨리 성장하고 있는지에 대한 모델을 잘 세웠다고도 할 수 있다. Defect Depth Growth rate 모델, 즉 External Corrosion rate 에 대한 예측모델 역시 많은 연구가 있어왔다. Defect Depth 와 마찬가지로 여러 환경변수의 영향을 받으므로, 이 역시 일반적인 예측을 위해 Adaptive 모델이 효과적이었다.

따라서 이를 통해 수소 충전소의 안전한 설계 및 충전소 외부로 수소를 이송하는 배관의 신뢰도 측정을 위한 Defect Depth 의 보다 정확한 예측모델을 연구할 수 있었다. 사람이 인접한 곳의 수소 충전소를 대상으로 하여, 더욱 신중하고, 안전한 설계가 요구되는 수요처이며, 위 연구를 통해 안전한 수소 저장소 설치 및 관리가 될 것을 기대한다.

주요어: 수소, 정량적 위험도 분석(QRA), 신뢰도 분석, 몬테-카를로 시뮬레이션, 한계상태함수, 지하매설배관

학 번: 2014-21591

Contents

Abstract i

Contents xi

List of Tables iv

List of Figures iv

Chapter1. Introduction 1

1.1. Research motivation..... 1

Chapter2. Safe design for onsite hydrogen refueling station..... 5

2.1. Background 5

2.2. Process description 9

2.2.1. Hydrogen production process modeling 9

2.3. Quantitative risk assessment procedure 47

2.4. Layout of the hydrogen refueling station..... 50

2.5. Result and discussion..... 52

2.5.1. Risk assessment result before process modification 52

2.5.1. Proposed process modification for risk mitigation 70

2.6. Conclusion 74

Chapter3. Adaptive approach for estimation of pipeline corrosion defects via Bayesian inference 75

3.1. Introduction 75

3.2. Adaptive estimation of corrosion defect depth 81

3.2.1. Time-dependent GEV distribution for corrosion defect depth distribution..... 81

3.2.2. Adaptive estimation framework using Bayesian inference 84

3.3. Implementation 89

3.4. Visualization and discussion 93

3.4.1. Case 1 – Direct inspection..... 93

3.4.1. Case 2 – indirect inspection 96

3.4.1. Case 3 – sudden changes in hidden depth distribution 100

3.5. Conclusion 108

Chapter4. Concluding remarks 110

Reference 112

List of Tables

2.1. Typical NGL feedstock composition 16

2.2. The condition of reaction 20

2.3. Verification 26

2.4. 2-stage Suction pressure specification according to the mass flow of the diaphragm compressor – First stage 31

2.5. 2-stage Suction pressure specification according to the mass flow of the diaphragm compressor – Second stage 32

2.6. Liquid gas petroleum composition 42

2.7. Reaction summary 46

3.1. Tested verification cases of corrosion depth estimation 92

List of Figures

2.1. PFD of tube trailer process 10

2.2. PFD of NG steam reforming process 14

2.3. Methane conversion or reforming efficiency depending on reforming temperature of SMR 22

2.4. Methane conversion or reforming efficiency and outlet concentration depending on steam to carbon ratio of SMR feed.....24

2.5. H2 recovery rate and CO concentration graph of product gas.. 29

2.6. Graph of Joule-Thompson coefficient according to pressure and temperature 34

2.7. Influence of the inlet gas temperature on the SoC for different filling rates..... 36

2.8. Solid-liquid phase diagram for ethylene glycol + water..... 39

2.9. PFD of LPG steam reforming process..... 40

2.10. Procedure of Risk assessment 49

2.11. Layout of hydrogen refueling station..... 51

2.12. QRA modeling & GIS input of Tube-trailer process 54

2.13. QRA result of Tube-trailer process (Societal Risk)..... 55

2.14. QRA result of Tube-trailer process (Individual Risk)..... 56

2.15. Sorting the unit and failure with descending order of risk results in tube-trailer case..... 57

2.16. QRA modeling & GIS input of NG steam reforming process..... 59

2.18. QRA result of NG reforming process (Societal Risk) 60

2.18. QRA result of NG reforming process (Individual Risk)..... 61

2.19. Sorting the unit and failure with descending order of risk results in NG reforming case 62

2.20. QRA modeling & GIS input of LPG steam reforming process 64

2.21. QRA result of LPG reforming process (Societal Risk) 65

2.22. QRA result of LPG reforming process (Individual Risk) .. 66

2.23. Sorting the unit and failure with descending order of risk

results in LPG reforming case. 67

2.24. Societal risk results from the three process 69

2.25. Risk mitigation result from NG process by reducing frequency of major 2 units. 72

2.26. Risk mitigation result from NG process by reducing frequency of major 5 units. 73

3.1. Pseudo code for adaptive estimation of corrosion depth distribution via Bayesian approach 88

3.2. Corrosion depth distribution results for Case 1..... 94

3.3. Corrosion depth distribution results for Case 2..... 96

3.4. Posterior distribution of coefficient estimation for Case 2. ... 99

3.5. Corrosion depth distribution results for Case 3..... 102

3.6. Posterior distribution of coefficient estimation for Case 3 .. 104

CHAPTER 1. Introduction

1.1. Research motivation

International demand for hydrogen is increasing. In particular, after the spread of electric vehicles, hydrogen has been connected not only with chemical plants, but also with people's living life. In this paper, the safe design of a hydrogen refueling station for electronic vehicle and the prediction of the corrosion damage of a pipe defect for the safe management of a hydrogen underground buried pipe is studied.

First, the safe design of a hydrogen refueling station targets a process that produces hydrogen from natural gas-derived material, which is known to be the most economical. This is a comparison of three processes: the first is to load hydrogen produced from the outside of the station carried by a high-pressure trailer, and then transform its pressure to meet the demand. The second is to produce hydrogen from gaseous NG(natural gas) through steam reforming

reaction, and the last is the process of producing hydrogen by steam reforming reaction through LPG.

All three processes is found to exceed tolerable risk levels in areas with some population density under currently known process conditions. Therefore, it is possible to safely design the process by changing the conditions of the process units that most affect the risk to mitigate the risk, or lower the frequency of failure event occurring by constructing additional firewalls.

On the other hand, off-site pipelines placed to transport the produced hydrogen going out of the hydrogen station or the incoming hydrogen from the outside are mainly installed in a buried form. Buried piping is an inevitable structure for the utilization of the ground area, but it is difficult to check the condition frequently due to the limitations of drilling costs and human resources to directly check the condition of the piping. Therefore, more attention should be paid to safety management. In particular, buried piping accidents in areas

close to the population, such as Kaohsiung in Taiwan or San Bruno in the United States, can cause personal injury, so evaluate and predict whether the risk or reliability of piping is safe and secure in the future. It is important to do.

There have been many studies predicting the defect depth distribution of pipes due to external corrosion. Predictive modeling of the previous papers were well predicted defect depths measured in the soil environments. However, the external corrosion of piping is affected by various environmental factors, so a well-made model may be inaccurate in other environments. This is because a large amount of data is required and it is generally difficult to apply to changing soils. To overcome this, the Adaptive Bayesian methodology is needed.

Predicting Defect Depth well can be said to have established a model for how quickly the defect depth is growing. Defect Depth Growth rate model, that is, prediction model for External Corrosion rate, has also been studied. Like Defect Depth, since it is affected by various

environmental variables, the Adaptive model is effective for general prediction.

Therefore, through this, it was possible to study a more accurate prediction model of the defect depth for the safe design of the hydrogen filling station and the reliability measurement of the pipe that transports hydrogen to the outside of the filling station. It is a demand for a more careful and safe design for the hydrogen charging station in the vicinity of a person, and it is expected that through the above study, a safe hydrogen storage will be installed and managed.

CHAPTER 2. Safe design for onsite hydrogen refueling station

2.1. Background

Hydrogen has been a promising eco-friendly energy source to replace existing fossil fuels and serve as a next-generation energy carrier. According to a recent International Energy Association (IEA) report, a variety of strategic roadmaps exists in each country for the construction of a hydrogen energy network, which will increase demand for hydrogen and reduce production costs in hydrogen production (IEA 2019). Hydrogen is produced through electrolysis, natural gas reforming, and coal gasification, and stored as high-pressure gas, liquefied and liquid compounds, and metal hydrogen compounds. An advantage of the liquid hydrogen type, when compared to compressed hydrogen, is that it operates at a lower pressure and can be efficiently stored in large amounts through a simpler process. However, it is important to consider safety when

using liquid hydrogen. This is because liquid hydrogen fueling stations are generally located in the center of densely populated cities, which helps to efficiently charge fuel-cell vehicles. Hence, an appropriate risk analysis of fueling stations, in terms of its design, operation, and maintenance, since they operate at pressures of 350bar-700bar (Stolten 2014).

Researchers have analyzed the consequences of an accidental release of hydrogen at large-scale facilities using CFD modeling (Bauwens and Dorofeev 2014). Other researchers have developed a framework based on HyRAM methodology to conduct quantitative risk assessment and consequence analysis to assess the safety of hydrogen fueling stations (Groth and Hecht 2017). Li et al. (Zhiyong, Xiangmin et al. 2011) have analyzed the risks for fueling station personnel, customers, and third parties when considering the QRA uncertainty for large gaseous hydrogen fueling stations. Haugom and Friis-Hansen have also performed comparisons between traditional

QRA and their QRA risk-modelling based on a Bayesian network at hydrogen fueling stations (Haugom and Friis-Hansen 2011). Gye et al. have conducted a study on risk mitigation scenarios for urban hydrogen fueling stations (Gye, Seo et al. 2019). One limitation of the existing research is that they do not perform QRA considering the entire process from hydrogen production to the supplying of fueling stations in the liquid phase. Hence, there is a need for a comprehensive QRA that considers the entire process from hydrogen production to supply, which includes 1) the hydrogen production to LPG water gas shift reforming, 2) NG water gas shift reforming, and 3) the pressure conversion of hydrogen, transported by trailer.

This study performs a risk analysis of these three hydrogen production-and-supply processes, while analyzing major units and accidents contributing to the risks in each process. We compare the results of risk mitigation to not exceed the tolerable risk criteria and

suggest the safest process for each of the three processes at fixed hydrogen production capacities.

2.2. Process description

2.2.1. Hydrogen production process modeling

The off-site process model was modeled based on the hydrogen station in Yangjae-dong. It is a hydrogen charging station that has been operating since May 2010 and operates at 700 bar.

Case1. Hydrogen transported by tube-trailer

■ Feed condition

① Tube trailer

The tube trailer is an important equipment that plays a role of storing and transporting by-product hydrogen produced in petrochemical complexes such as Ulsan and Yeosu as a hydrogen filling station. The hydrogen tube trailer compresses and stores high-purity hydrogen at 200 bar and supplies it to the hydrogen filling station.

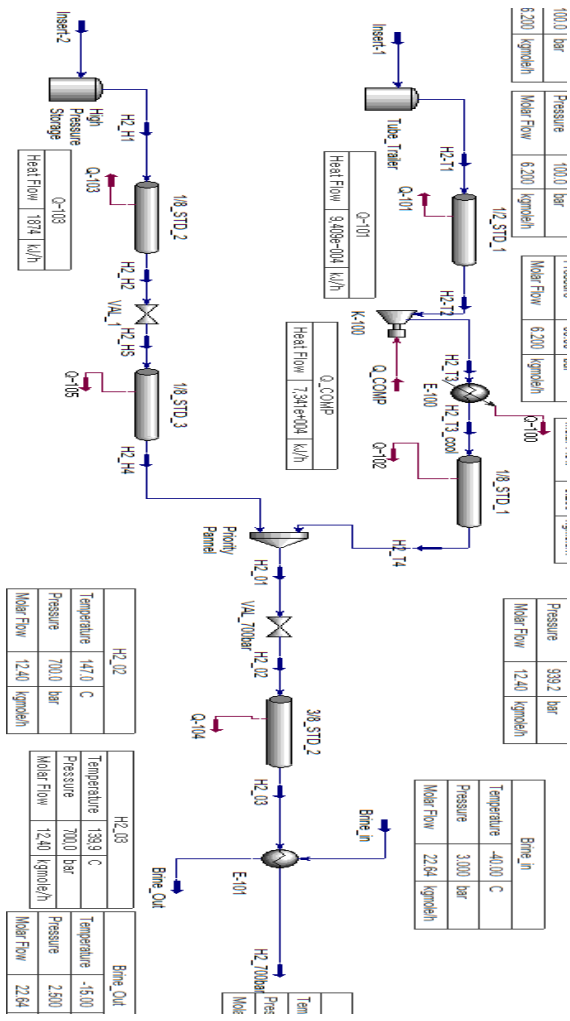

Figure 2.1. PFD of tube trailer process

② High pressure hydrogen storage tank

The tank pressure of a conventional hydrogen vehicle is 350 bar, and the pressure of a hydrogen fueling station storing hydrogen is 400 bar. Therefore, the pressure of the station is 1.1+α times higher than that of the vehicle tank, and this is used as the driving pressure. That is, in this study, the pressure supplied to the hydrogen vehicle is 700 bar, and the pressure of the high pressure hydrogen storage tank is 800 bar.

A. Main units.

① Compressor

The station at Yangjae Station supplies fuel to the hydrogen vehicle at 700 bar. Since the pressure supplied to the tube trailer is 200 bar, it is pressurized to 800 bar with a compressor.② Valve+700bar

Since the pressure supplied to the hydrogen vehicle is supplied at 1.1+α times, the pressure of the tank pressurized to 800bar must be reduced to 700bar. After that, the refrigerant is supplied to the hydrogen vehicle at -40°C.

■ Plant capacity

The flow rate of the hydrogen product is 600 kg/day. This figure assumes a 24-hour operation for the 25 kg_H2/h specification of the hydrogen charging station (“Anseong hydrogen charging station”) currently built by Hyundai Motor Company.■ Feed condition

City gas composition was used for the composition of Lean gas from 'Equipment Design and Cost Estimation for Small Modular Biomass Systems, Synthesis Gas Cleanup, and Oxygen Separation Equipment / Table 2.1. below. In addition, odorants added to city gas include tertiary-butyl-mercaptan (TBM) and tetra-hydro-thiophene

(THT) at a ratio of 30:70% (about 4ppm / 20mg/Nm3_NG), respectively.

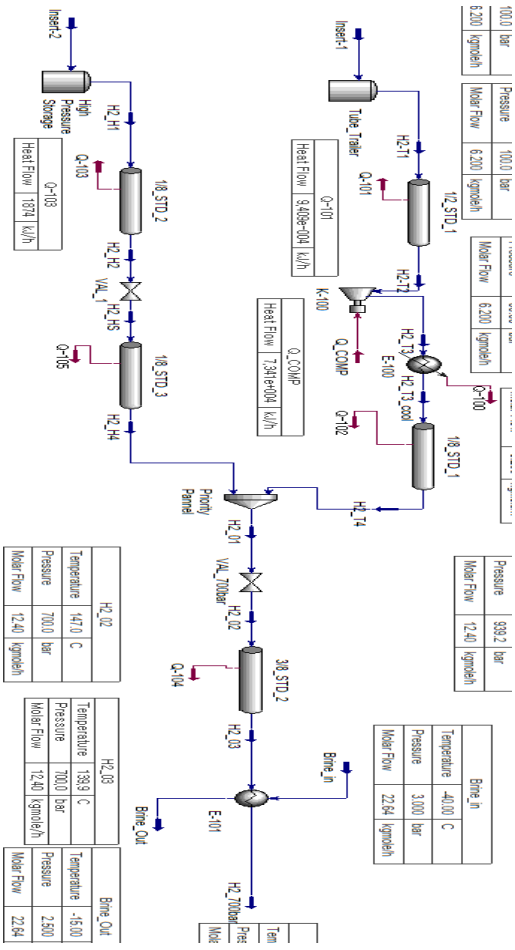

Figure 2.2. PFD of NG steam reforming process

Case2. Natural gas steam reforming process

The city gas supply pressure can be supplied below the maximum pressure of 4Mpa according to the ‘City Gas Supply Regulations Article 26 Paragraph 1’, so the supply pressure was applied considering the reaction pressure and the pressure drop value.

Table 2.1. Typical NGL Feedstock Compositions

	Classification			
	Super-Rich	Rich	Lean	Super-Lean
C1 (mole%)	82.00	87.00	92.00	96.30
C2	9.70	7.90	4.80	2.20
C3	4.50	3.30	1.80	0.80
IC4	0.50	0.46	0.49	0.20
NC4	1.80	1.13	0.87	0.50
IC5	0.50	0.00	0.00	0.00
NC5	0.49	0.21	0.04	0.00
C6+	0.51	0.00	0.00	0.00
BTU/scf	1251.81	1161.77	1105.35	1054.51

A. Main units.

① Desulfurization

The odorant added to city gas contains tertiary-butyl-mercaptan (TBM) and tetra-hydro-thiophene (THT) at a ratio of 30:70% (about 4 ppm), respectively. Both of these odorant components are sulfur-containing compounds, which act as catalyst poisons to the catalyst in the reformer for producing hydrogen from natural gas, thereby deteriorating the durability of the catalyst and adversely affecting hydrogen productivity. Therefore, it is necessary to supply the concentration of sulfur component below 10 ppb.

The desulfurization method is largely divided into a hydrogenation desulfurization method and a room temperature desulfurization method. The hydrogenation desulfurization method has excellent desulfurization performance, but the system is complex, the reactor size is large, and 350℃, because it needs to separate and adsorb the

sulfur component through a chemical reaction. The above reaction temperature is required, so it is suitable for large systems, but it is difficult to apply to small systems such as on-site hydrogen stations. Therefore, a room temperature desulfurization method using a desulfurization adsorbent capable of separating and removing sulfur compounds through adsorption at room temperature was applied.

According to the selective adsorption and removal of sulfur compounds deposited in LNG gas on a metal-containing beta zeolite adsorbent,' the adsorbent supported by the combination of metals under the condition that the Cu/Zn ratio is 2 and the Fe/Mo ratio is 3 is the highest in the beta zeolite. It showed the ability to adsorb and remove odorants. In this process, the device is simulated using a simple component splitter.

② NG reforming

The main reaction formula of the natural gas reforming reaction is as follows.

a. Steam Methane Reforming reaction

$$\mathrm{CH_4} + H_2O \leftrightarrow 3H_2 + CO \qquad \Delta H_{298}^0 = -206.28\frac{kJ}{mol}$$

$$\mathrm{CH_4} + 2H_2O \leftrightarrow CO_2 + 4H_2 \qquad \Delta H_{298}^0 = 165\frac{kJ}{mol}$$

b. Water Gas Shift reaction

$$\mathrm{CO} + \mathrm{H_2}O \leftrightarrow CO_2 + H_2 \qquad \Delta H_{298}^0 = -41.2\frac{kJ}{mol}$$

The reaction-related conditions for each reaction are shown in Table 2. 2.

Table 2.2. The condition of reaction

Reaction type	Temperature (°C)	Pressure (bar)	Catalyst
SMR reaction	716.8	1.4	Ni/Al2O3
WGS reaction	290	1.3	Cu/ZnO/Al2O3

Figure 2.3. is a graph of experimental values for methane conversion and reforming efficiency according to the reforming temperature of the SMR reaction.

The equation for the reforming efficiency is as follows.

$$\eta = \frac{LHV_{product}}{E_{input} + LHV_{feed}}$$

LHV : Lower Heating Value

According to Figure 2.3., the higher the reaction temperature, the lower the equilibrium conversion rate and deviation, and there is no significant difference in methane conversion rate and reforming efficiency. The larger the reaction temperature, the greater the methane conversion rate, but the greater the energy required to meet the reaction temperature, the higher the concentration of CO, the product, and there is a tradeoff relationship between the load and reactor durability of the subsequent WGS reactor. Therefore, in this process, 700~720°C was set to an appropriate reforming temperature.

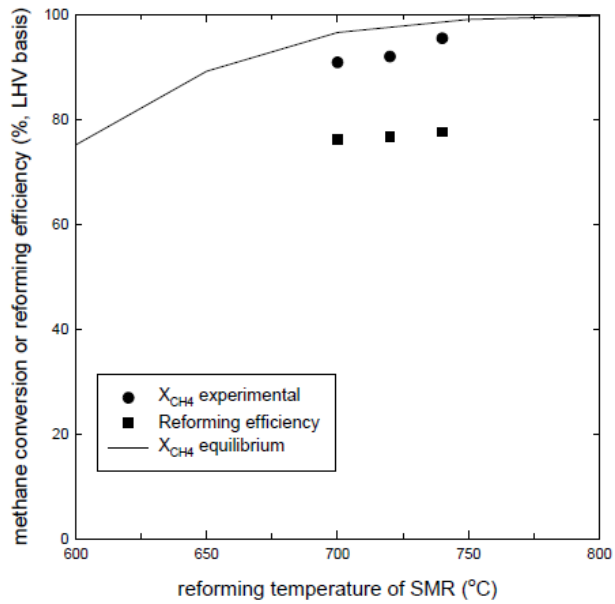

Figure 2.3 Methane conversion or reforming efficiency depending on reforming temperature of SMR

Figure 2.4. is a graph of methane conversion or reforming efficiency and methane and CO concentration according to the water/methane ratio of the SMR reactant. As the water vapor/methane ratio increased, the methane conversion rate increased and the CO concentration at the exit of the WGS reactor decreased, but at the same time, the amount of supplied water vapor for the amount of methane increased, so there was no significant change in reforming efficiency due to the increase in power consumption. Therefore, 3 was set as the proper water vapor/methane ratio.

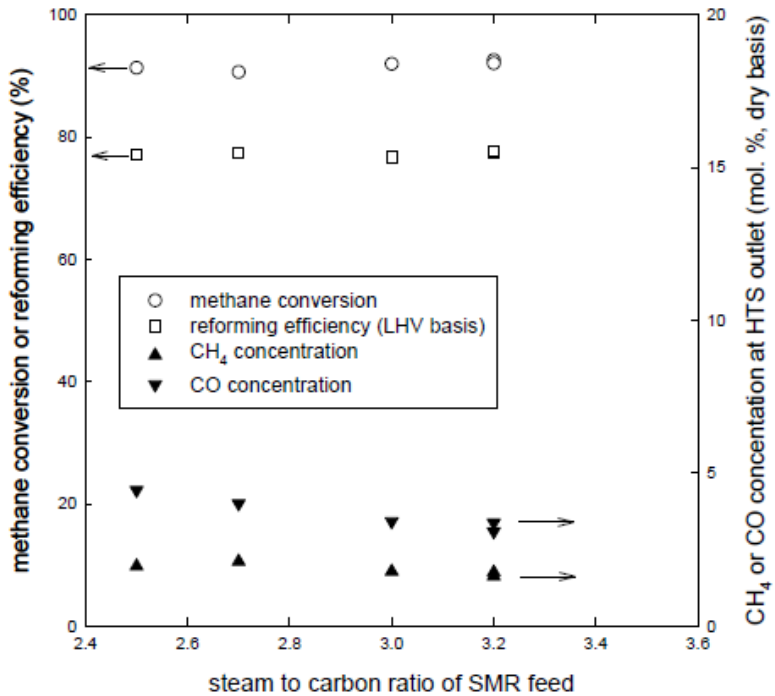

Figure 2.4. Methane conversion or reforming efficiency and outlet concentration depending on steam to carbon ratio of SMR feed

The simulation results for this process were verified by comparing with the actual process data actual process data.

Table 2.3. Verifications

	Feed consumption	**Energy consumption**	**Reforming efficiency***
Units	($\mathrm{Nm3_{NG}}/Nm3_{H2}$)	($kWh/Nm3_{H2}$)	(%, LHV)
This model	0.382	1.29	51
KIER-1	0.384	1.07	56.7
KIER-2	0.378	0.997	58.1
Osaka Gas	0.358	0.756	61.3
WE-NET	0.357	0.915	59.5

③ PSA(Pressure Swing Adsorption)

Hydrogen reformed from natural gas includes CO, CO2, and CH4, of which carbon monoxide reacts with the catalyst of the fuel cell to degrade the performance and durability of the fuel cell. Therefore, more than 99.995% high purity hydrogen is required to maintain the performance and life of the fuel cell.

The PSA process is a process of removing components such as CO2, CO, N2, and unreacted CH4 in order to increase the concentration of hydrogen as a target product among reaction products. The PSA process is based on the principle that a gas with high selectivity, such as carbon dioxide, is first adsorbed while a mixed gas passes through the adsorption tower filled with the adsorbent under high pressure, and the hydrogen gas with low selectivity is discharged out of the adsorption tower. The operating temperature and pressure of the PSA process are 40 and 9.2 bar, respectively. Compression was performed

using a reciprocating compressor to match the corresponding operating conditions.

Figure 2.5. shows the H2 recovery rate for the CO concentration of the raw material gas and the CO concentration graph of the product gas. In this process, the CO concentration of the raw material gas was measured at 2.7 mol (%), and the corresponding H2 recovery rate (70%) was applied to simulate the component splitter.

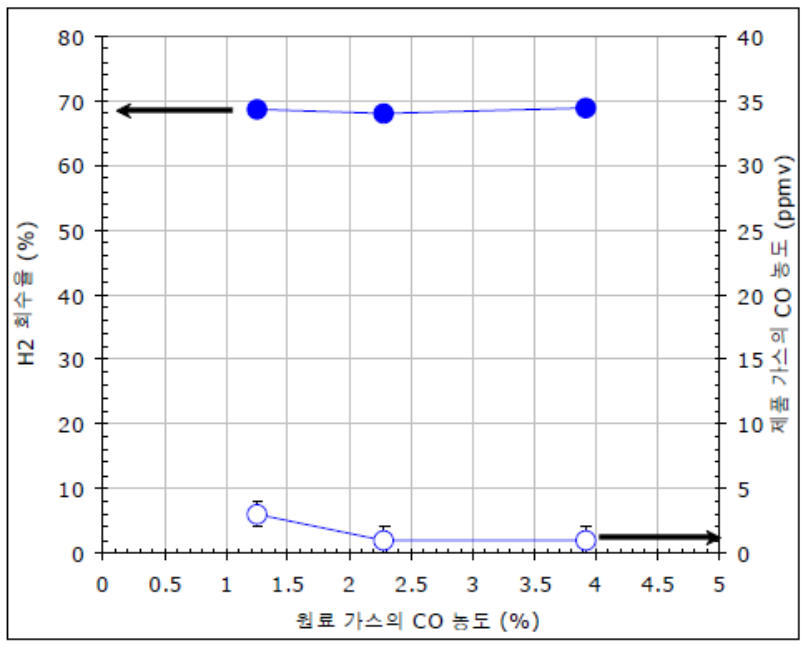

Figure 5. H_2 recovery rate and CO concentration graph of product gas

④ Compression

In order to efficiently store hydrogen in a hydrogen tank, it must be compressed at a high pressure of 950 bar. The compressor used in the process generally used a diaphragm compressor that is frequently used for hydrogen compression, and the suction pressure of the diaphragm compressor was simulated through a reciprocating compressor. The table below shows the detailed specifications of the 2-stage diaphragm compressor.

Table 2.4. 2-stage Suction pressure specification according to the mass flow of the diaphragm compressor – First stage

First stage capacity : Discharge 500bar					
Suction Pressure(PSIG)	5,816	4,350	2,900	1,450	725
Suction Pressure (bar)	401	300	200	100	50
Mass Flow (Nm^3/hr)	1,420	1,079	750	400	200
Kg/h	128	97	67	36	18
Kg/d (max)	3,062	2,327	1,618	863	431

Table 2.5. 2-stage Suction pressure specification according to the mass flow of the diaphragm compressor – Second stage

Second stage capacity : Discharge 950 bar				
Suction Pressure (PSIG)	7,500	7,250	5,800	4,350
Suction Pressure (bar)	517	500	400	300
Mass Flow (Nm^3/hr)	811	790	700	500
Kg/h	73	71	63	45
Kg/d (max)	1,750	1,704	1,510	1,079

⑤ Cooling system

Since there is a significant increase in the temperature of the gas during refueling, hydrogen must be cooled before filling the vehicle with hydrogen. There are three main reasons for explaining this temperature increase.

1. The temperature is increased by the Joule-Thomson effect.

The pressure drop occurs when hydrogen gas is put into the vehicle through the dispenser, where the Joule Thompson effect is applied. The Joule Thompson effect represents the temperature change that occurs when compressed gas is ejected into an insulated narrow hole. Quantitative indicators of the effect are as follows.

* Joule-Thomson coefficient $\mu_{JT} = \left(\frac{\partial T}{\partial P}\right)_H$

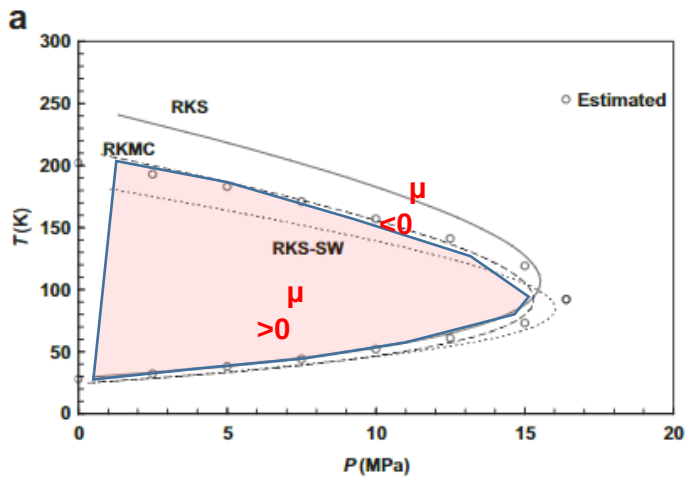

Figure 2.6 Graph of Joule-Thompson coefficient according to pressure and temperature

According to Figure 2.6., the area colored in pink has a positive Joule Thompson coefficient. Therefore, the lower the pressure, the lower the temperature. Since the pressure condition in this process is more than 150 bar, the Joule Thompson coefficient of the current condition is negative, so the temperature increases as the pressure decreases.

2. The kinetic energy of hydrogen gas is converted into the energy inside the hydrogen tank.

3. The temperature rises as the gas inside the hydrogen tank is compressed by the high pressure gas supplied.

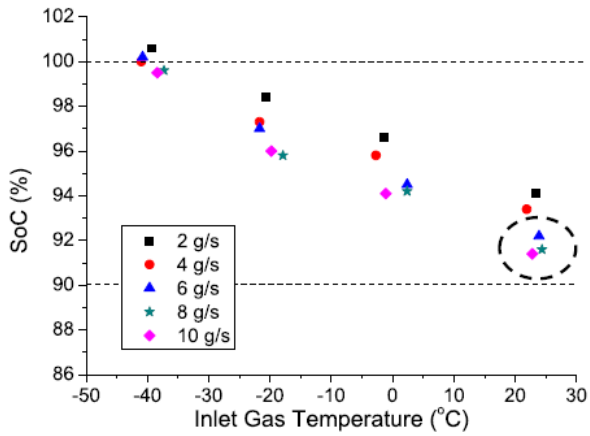

Figure 2.7. Influence of the inlet gas temperature on the SoC for different filling rates

*SoC : Storage of Charge

Figure 2.7. is a graph showing SoC according to the inlet gas temperature for the gas filling speed. SoC (0% = empty; 100% = full) is an indicator of how much hydrogen gas is charged in the vehicle. It can be seen that at an inlet gas temperature of -40 to -30°C, the SoC is near 100%, and as the temperature increases, the SoC decreases. The dashed-line in the figure may cause stability problems when the inlet gas flows into the hydrogen tank tank at 20~30°C, and the gas temperature exceeds 85°C. Therefore, an appropriate cooling temperature was set to -40.

There are two methods of cooling system design: direct cooling system and indirect cooling system. The direct cooling method is a method of directly transferring the heat source of the refrigerant to the precooler, and the indirect cooling method is a method of transferring the heat source of the refrigerant to the precooler through the secondary refrigerant. In the case of the hydrogen station currently being built, an indirect cooling method is adopted for safety reasons.

The refrigerant must supply a cold heat source for the purpose of cooling hydrogen to -40 degrees, so R507, which has a boiling point of -46.7 degrees at atmospheric pressure, a large evaporation latent heat, and a low warming coefficient, is used as the refrigerant. In addition, ethylene glycol water was used as the secondary refrigerant. As shown in Figure 2.8., the weight composition with the lowest freezing point of EG was 60 wt%.

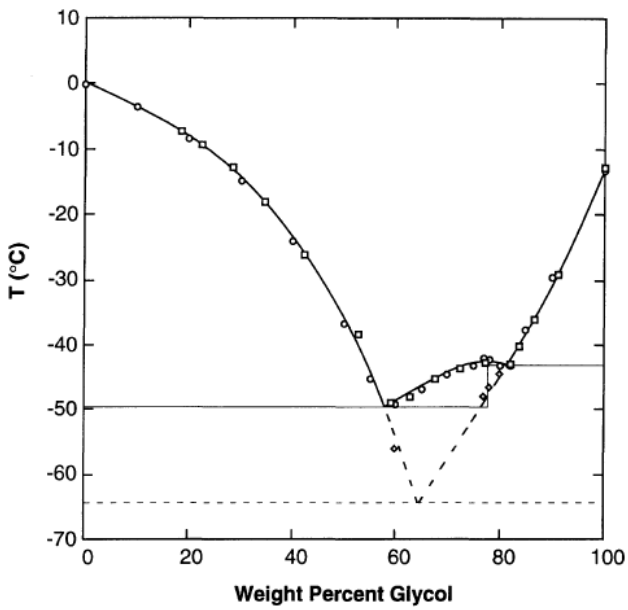

Figure 2. Solid-liquid phase diagram for ethylene glycol + water. ○ : stable freezing points, Lab 1; □ : stable freezing points, Lab 2; ◇ : metastable freezing points, Lab 1; — : average stable freezing curve; - - : metastable freezing curve.

Figure 2.8 Solid-liquid phase diagram for ethylene glycol + water

Case3. LPG steam reforming process

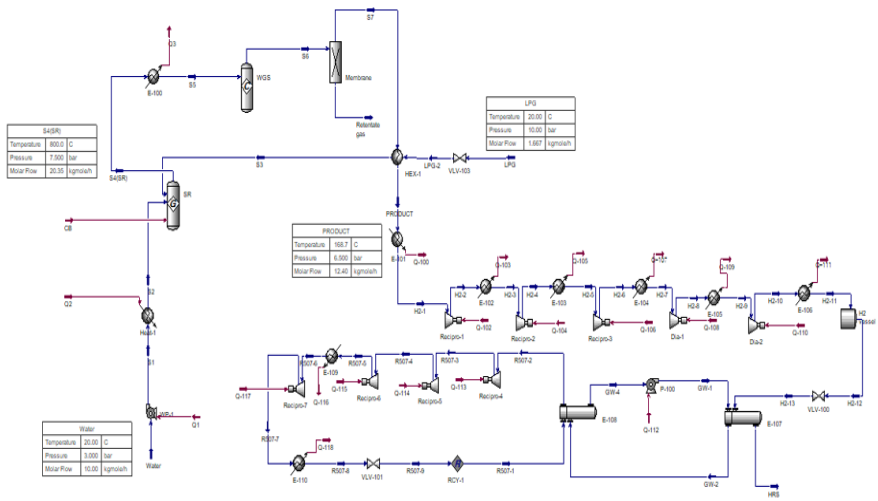

Figure 2.9. PFD of LPG steam reforming process

■ Plant capacity

Plant capacity is based on 600kg/d. In fact, at the Hydrogen refueling station operated at Anseong Rest Area, it has a charging capacity of 25kg/h that can buffer more than 5 hydrogen vehicles per hour. When this charging station is operated for 24 hours, it can have a charging capacity of 600 kg/d.■ Feed condition

① LPG

LPG consists of hydrocarbons. It is mainly a mixture of propane and n-butane, and its composition is different depending on the process and season. In fact, the Korea National Oil Commission regulates the ratio of propane in summer and winter according to the liquefied petroleum gas safety management and business law. In the summer, the proportion of propane is controlled to less than 10 mol%, and in the winter, the proportion of propane is controlled to 25 to 35%. Table X+1 shows the LPG composition considered in this study.

Table 2.1. Liquid gas petroleum composition

Liquid gas petroleum composition (mol %)		
Propane (C_3H_8)	%	84.0
n-Butane (C_4H_{10})	%	12.9
Ethane (C_2H_6)	%	3.1
Heating values		
	MJ/kg	MJ/Nm^3
HHV	50.3	93.4
LHV	46.3	86.1

In addition, LPG exists as a gas at atmospheric pressure of about 20℃, but when a pressure of 6 bar or more is applied, it becomes a liquid. In the national standard NFPA58, LPG is stored at 54.4℃ at 7 bar.

② water

According to KDS 57 65 00 of the National Construction Standards Center in Korea, the water supply is designed to have a water pressure of 1.5 bar to 7.0 bar. At this time, the water pressure supplied to the home is 3 bar.

A. Main units.

① LPG Stream Reforming

Experimental studies show examples that can be represented in LPG reforming reaction systems. This reaction is endothermic and is preferred at around 700-800°C.

Reaction 3.1 $C_4H_{10} + H_2O \leftrightarrow C_3H_8 + CO + 2\ H_2$

Reaction 3.2 $C_3H_8 + H_2O \leftrightarrow C_2H_6 + CO + 2H_2$

Reaction 3.3 $C_2H_6 + H_2O \leftrightarrow CH_4 + CO + 2H_2$

Reaction 3.4 $C_2H_4 + H_2O \leftrightarrow CH_4 + CO + H_2$

Reaction 3.5 $CH_4 + H_2O \leftrightarrow CO + 3H_2$

Reaction 3.6 $CO + H_2O \leftrightarrow CO_2 + H_2$

Reaction 3.7 $CO + H_2 \leftrightarrow C(s) + H_2O$

The catalyst uses $LaNiO_3$, the optimum reaction temperature is 800℃ and the pressure is 7.5bar. The S/C molar ratio is selected as 6.

③ Membrane shift reaction, MSR

MSR is a model that combines WGS reaction and hydrogen purification process. WGS is used to make more hydrogen by reacting carbon monoxide and water in syngas. In order to simulate this reaction, a separation process and a WGS model were separately implemented. The hydrogen molecule thus generated is dissociated

into a hydrogen reactor at the supply side of the film, then diffused through the film and reconnected at the transmission side.

Reaction 4.1$CO + H_2O = CO_2 + 2H_2$

The catalyst uses Pd-Ag, the optimum pressure is 7 bar, and the reaction temperature is 350°C. This reaction is exothermic and the temperature rises after the reaction. The results obtained from the model were verified by comparing them with experimental data. The reaction was summarized in Table 3.6 .

Table 2.2. Reaction summary

Reaction	Catalyst	Temperature	Pressure
Steam reaction	LaNiO3	800°C	6.5bar
Water gas shift	Pd-Ag	350°C	7bar

2.3. Quantitative risk assessment procedure

The risk was analyzed through the most common quantitative risk assessment (QRA). (Figure 2.10.)The first step is Hazard Identification, which is not a risk analysis for units in all processes, but a step to focus on analyzing which units are hazards that cause hazards in the process and to analyze the risks for the units.

Next step is scenario selection, which predicts what kind of accident will happen in the unit identified by Hazard Identification. It is a step to predict which Failure will occur and which event will be the final event.

Then there are Consequence Analysis, which predicts the size of an accident when it occurs, and Frequency Analysis, which predicts how often an accident will occur.

Then, the results of each step are combined to determine whether the process to be analyzed satisfies the socially acceptable level of risk.

Here, if the risk exceeds the Tolerable Risk Level, the process must perform risk mitigation to lower the risk level.

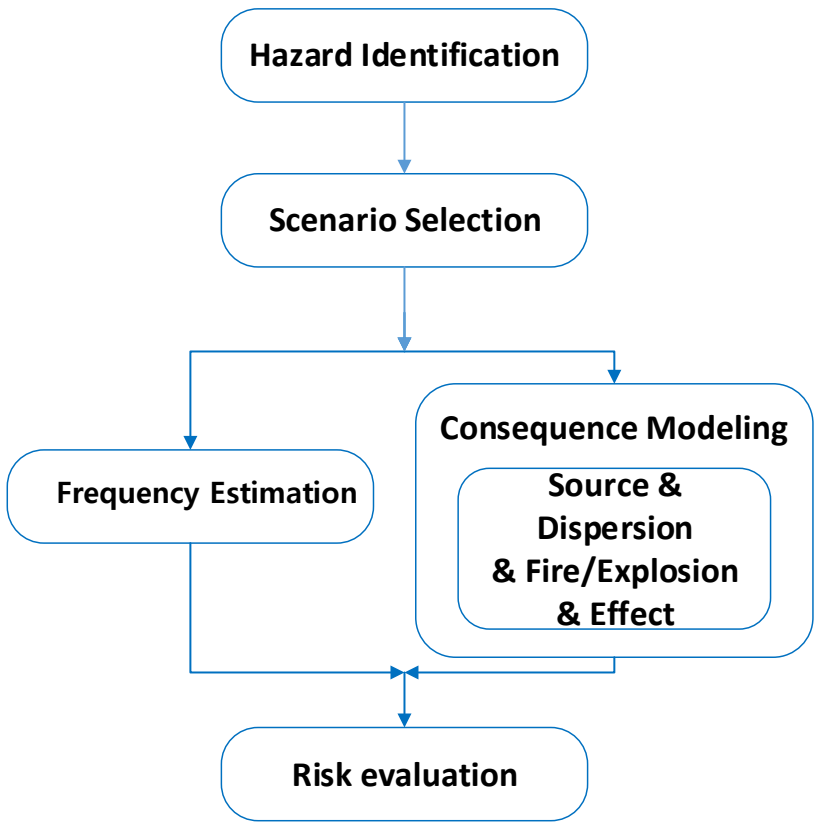

Figure 2.10. Procedure of Risk assessment

2.4. Layout of the hydrogen refueling station

Figure 2.11. is a hydrogen refueling station located in the city, the subject of this study. To simplify the analysis, there is one operating room, a chiller for cooling the hydrogen near the operating room, one process building, tube-trailer for hydrogen transport, and surrounding residential areas and highways.

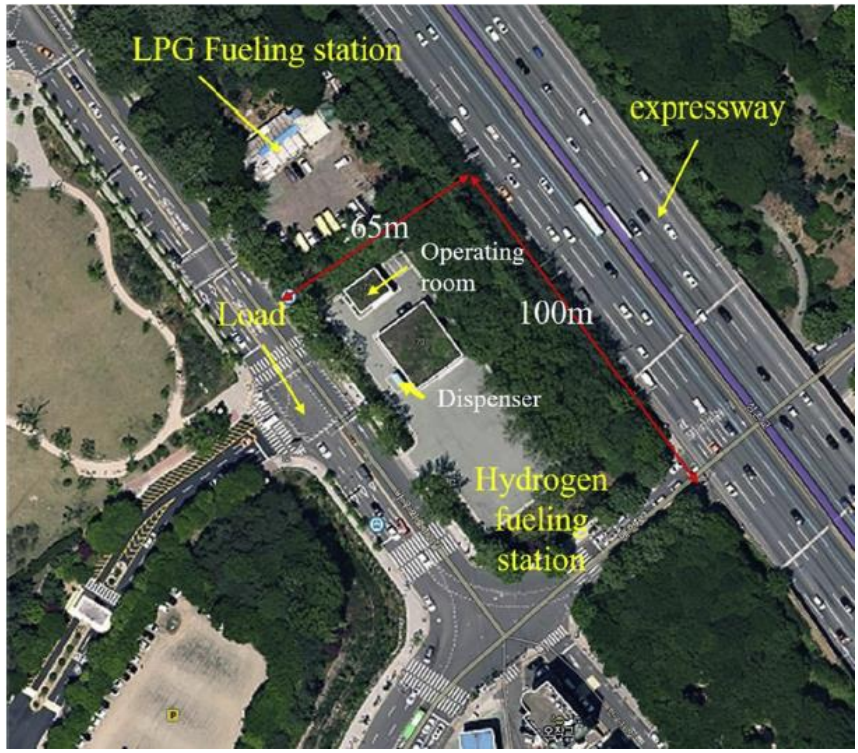

Figure 2.11. Layout of hydrogen refueling station

2.5. Result and discussion

2.5.1.Risk assessment result before process modification

For the modeling of the process, Aspen Hysys and Risk Assessment used PHAST and SAFETI, which are commercially available risk analysis programs.

Case1. Hydrogen transported by tube-trailer.

Figure 2.12. shows the unit type and location of the analysis target entered in SAFETI, and the topographic information of the highways and residential areas, which are the densely populated areas. The results of this analysis can be confirmed in Figure 2.13. and Figure 2.14. In Figure 2.13., it can be seen that the red line, which is the level of tolerable risk, was crossed. Also, in Figure 2.14., it can be seen that the unit's risk zone spans not only the process target area but also the

surrounding off-site. Through this, it can be seen that the process needs to lower the risk.

In addition, in Figure 2.15., the rupture failure of the hydrogen storage and trailer is analyzed as the cause of the greatest risk.

Figure 2.12. QRA modeling & GIS input of Tube-trailer process

Figure 2.13. QRA result of Tube-trailer process (Societal Risk)

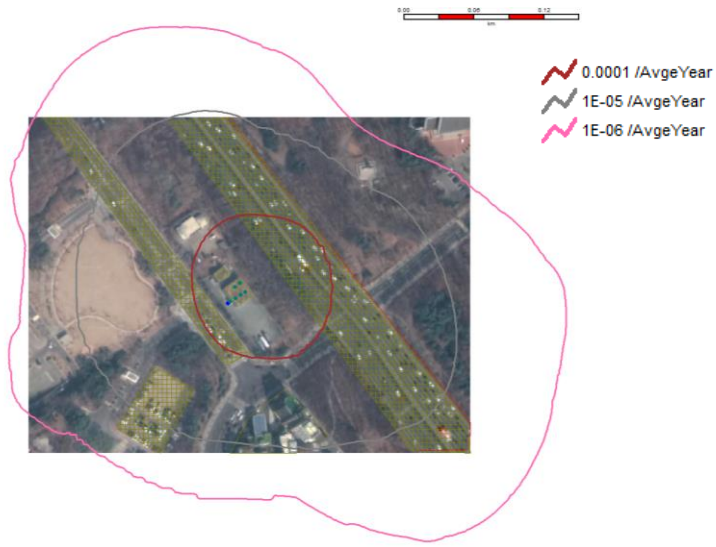

Figure 2.14. QRA result of Tube-trailer process (Individual Risk)

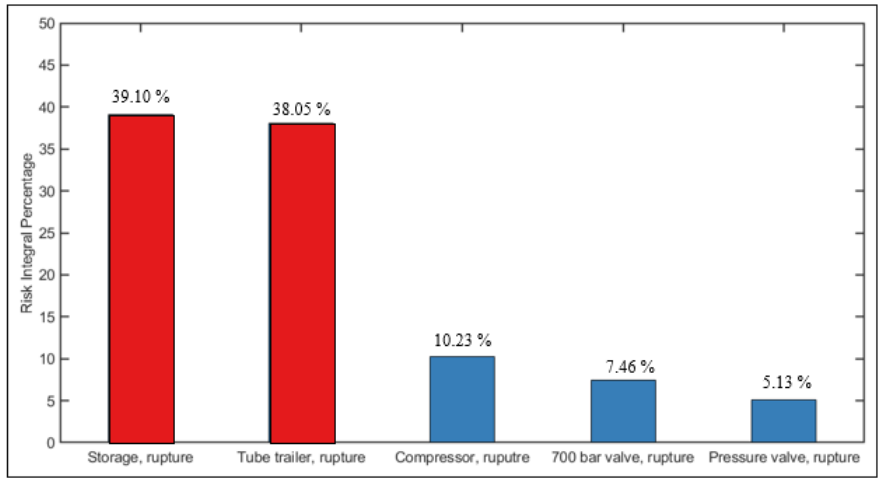

Figure 2.15. Sorting the unit and failure with descending order of risk results in tube-trailer case.

Case2. Natural gas steam reforming process

Figure2.16. shows the unit type and location of the analysis for NG steam reforming QRA, target entered in SAFETI, and the topographic information of the highways and residential areas, which are the densely populated areas. The results of this analysis can be confirmed in Figure2.17. and Figure2.18. In Figure2.17., it can be seen that the red line, which is the level of tolerable risk, was crossed. Also, in Figure 2.18., it can be seen that the unit's risk zone spans not only the process target area but also the surrounding off-site. Through this, it can be seen that the process needs to lower the risk, as in the previous result of tube-trailer case.

In addition, in Figure 2.19., the rupture failure of the desulfurizer and ERV is analyzed as the cause of the greatest risk.

Figure 2.16. QRA modeling & GIS input of NG steam reforming process

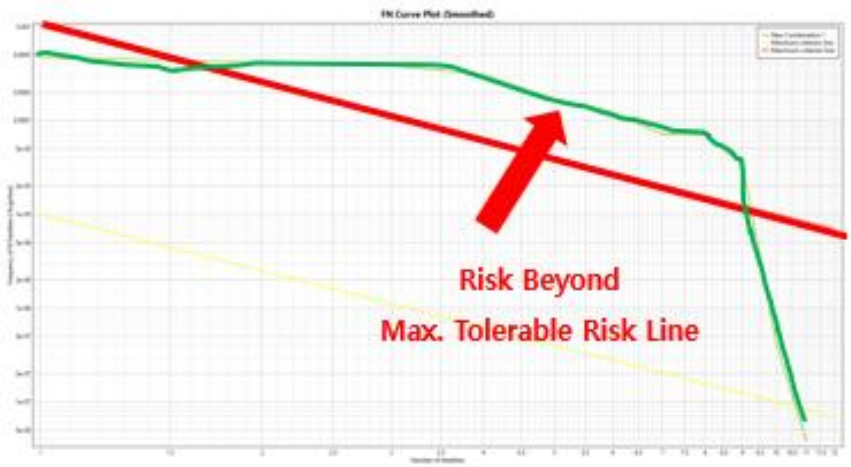

Figure 2.17 QRA result of NG reforming process (Societal Risk)

Figure 2.18. QRA result of NG reforming process (Individual Risk)

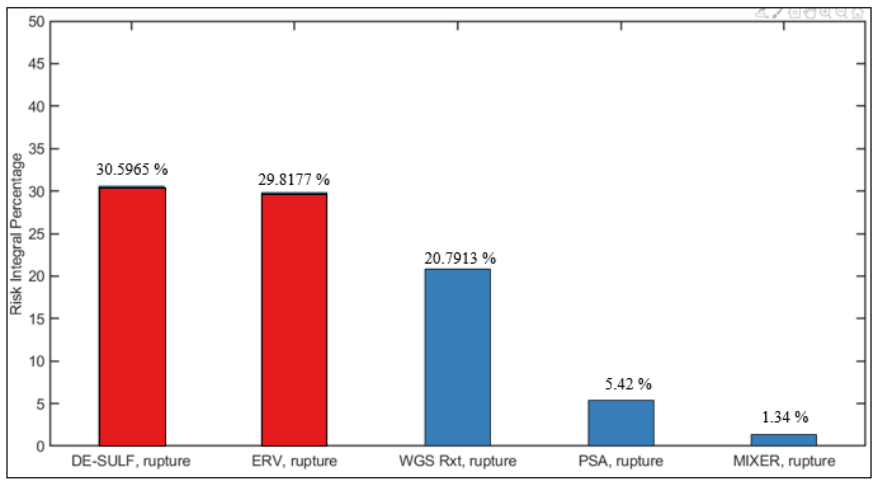

Figure 2.19. Sorting the unit and failure with descending order of risk results in NG reforming case.

Case3. LPG steam reforming process

Figure2.20. shows the unit type and location of the analysis for LPG steam reforming QRA, target entered in SAFETI, and the topographic information of the highways and residential areas, which are the densely populated areas. The results of this analysis can be confirmed in Figure2.21. and Figure2.22. In Figure2.21., it can be seen that the red line, which is the level of tolerable risk, was crossed. Also, in Figure 2.22., it can be seen that the unit's risk zone spans not only the process target area but also the surrounding off-site. Through this, it can be seen that the process needs to lower the risk, as in the previous results.

In addition, in Figure 2.23., the rupture failure of the E100(heat exchanger) and WGS reactor is analyzed as the cause of the greatest risk.

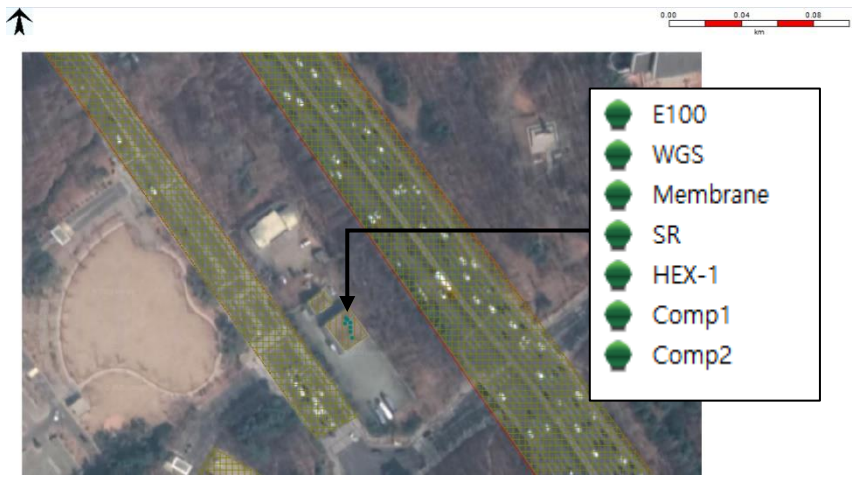

Figure 2.20. QRA modeling & GIS input of LPG steam reforming process

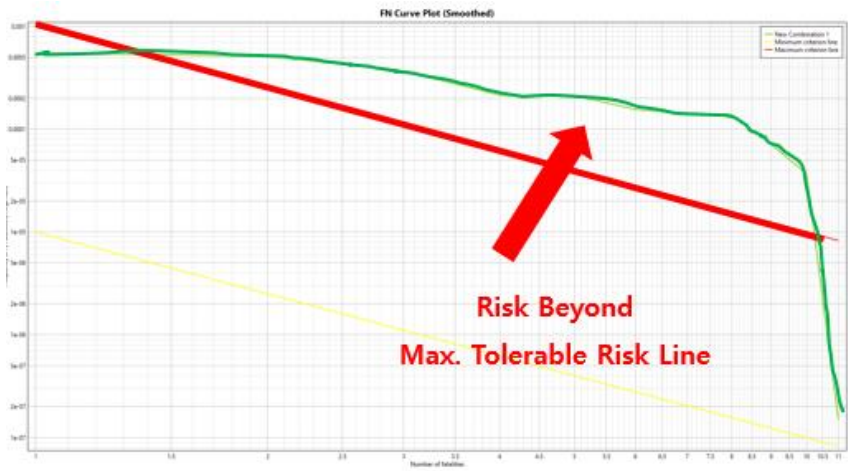

Figure 2.21. QRA result of LPG reforming process (Societal Risk)

Figure 2.22. QRA result of LPG reforming process (Individual Risk)

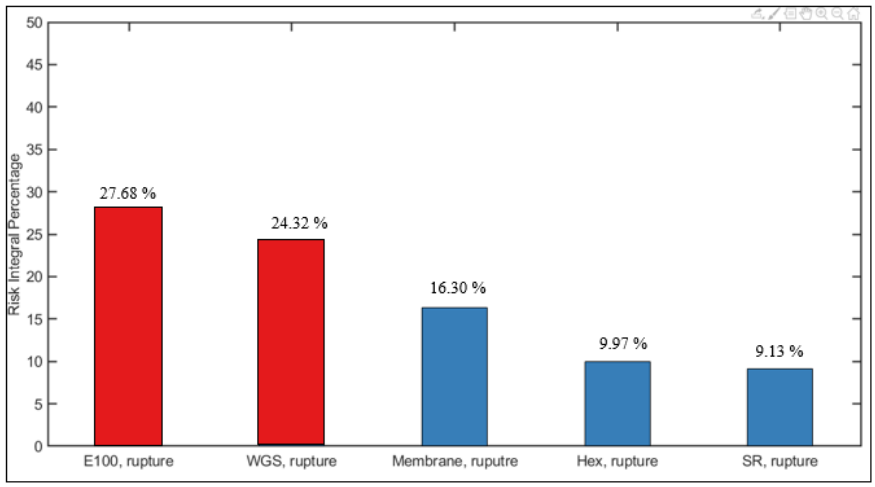

Figure 2.23. Sorting the unit and failure with descending order of risk results in LPG reforming case.

Since all the previous three processes exceeded the tolerance level, risk mitigation is required. The result of comparing the societal risks of the three processes can be seen in Figure 2.24. As a result, the NG steam reforming process was found to be the safest under the three current process conditions. After this, mitigation of the risk to the NG process is also performed. This is because, due to the analysis we made, reducing the risk in the NG process is the easiest way to achieve a tolerable risk level among the three process.

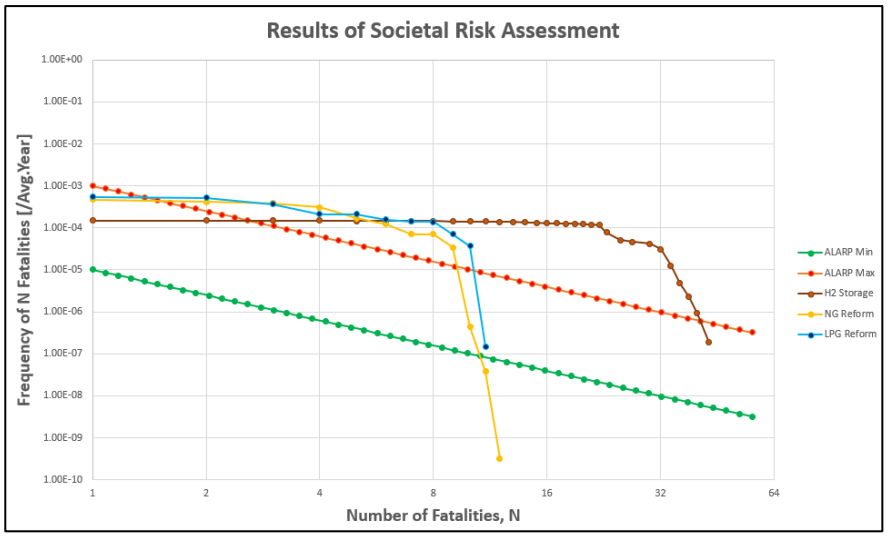

Figure 2.24. Societal risk results from the three process

2.5.2. Proposed process modification for risk mitigation

To reduce the risk of the process, there are two main methods. There are methods to reduce the size of accidents by adjusting the temperature, pressure and flow rate of the process to reduce the risk of accidents and leaks, and to reduce the frequency of accidents by improving the firewall and process control methods.

The first method is highly related to the capacity of the process. It is natural that the hourly output of a product changes when the temperature, pressure and flow rate change. Therefore, the second method, a method of reducing the risk by adjusting the frequency of accidents, is one of the simple and easy ways to lower the risk. Of course, there will be additional costs for firewalls, but a precise economic analysis would be nice if we could study it later. For simplicity of analysis, economic analysis is omitted here.

The risk of desulfurizer and E100 (Heat Exchanger) was the most dominant in the NG steam reforming process of 2.4.1. Therefore, the frequency of accidents between these two units was first lowered by installing a firewall. According to Gye(2019), the frequency is reduced by about 10^{-2}.

The results are shown in Figure 2.25. As can be seen, there are still cases where it is more dangerous than a tolerable level. Therefore, the frequency of accidents for the remaining three units analyzed in Figure 2.19. was also lowered and analyzed.

As a result of risk mitigation for Major 5 units, as shown in Figure 2.26., it was always possible to maintain a lower risk level than the Tolerable risk level.

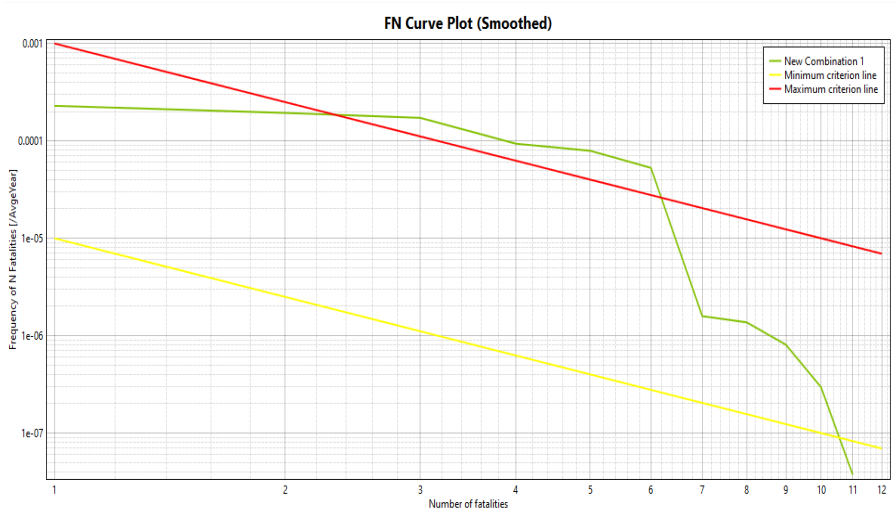

Figure 2.25. Risk mitigation result from NG process by reducing frequency of major 2 units.

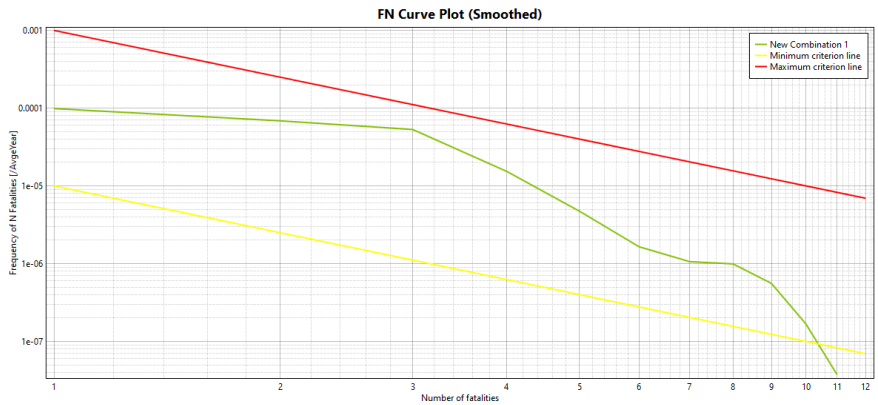

Figure 2.26. Risk mitigation result from NG process by reducing frequency of major 5 units.

2.6. Conclusion

Risk analysis is performed for three representative processes used in hydrogen charging stations, risk comparison was performed, and risk mitigation was performed for the natural gas steam reforming process, which was the easiest to reduce risk.

Through the analysis of risk contribution, major five units causing risk were identified and risk mitigation was conducted by reducing the frequency of accidents for the units.

Finally, the risk level of the process that is always below the level of tolerable risk. In the future, risks and mitigation will be meaningful considering weighting for the major five units mentioned and considering the size of the accident and economic capacity.

Chapter 3. Adaptive approach for estimation of pipeline corrosion defects via Bayesian inference

3.1 Introduction

Pipelines are essential elements of chemical and petrochemical plants to transfer fluids. Pipelines are often buried underground due to the limited area of construction sites, which in turn exposes the pipelines to the damages such as corrosion defects. As accidents caused by the defects left on pipelines can lead to economic disasters and casualties, a careful maintenance plan should be prepared. However, the defects on the underground pipelines are difficult to be detected owing to economic reasons, thus the inspection data is rare to construct an accurate model used to devise a maintenance plan. Indirect observation methods such as in-line inspection (ILI) are often employed to reduce the burden of inspection cost, but the data has inevitable measurement errors to be used for deterministic models and the amount of data still remain rate. Therefore, an efficient approach to construct the defect estimation model accurate enough to be employed for maintenance plan is

required(A.Gabbar and Kishawy 2011, Adetunji 2013, Gomes, Beck et al. 2013).

European Gas Pipeline Incident Data Group (EGIG) and Pipeline and Hazardous Materials Safety Administration (PHMSA) have reported that corrosion is indicated as the most frequent cause of the underground pipeline accidents among the time-dependent factors of pipeline accidents (EGIG). According to the report by Canada Standard Association (CSA), since the external corrosion of pipeline deepens the depth of defects, it lowers the maximum allowable operating pressure (MAOP), which in turn increases the risks of catastrophic events such as jet fire and flash fire from rupture failures. Thus, the maintenance plan for the corroding pipelines via accurate estimation of the defect depth should be attained to increase the reliability of pipelines(Chen and Wu 2015). Researchers derived several corrosion models related in corrosion depth and pit growth rate for performing reliability analysis of underground pipelines from both synthetic and field gathered corrosion data (Vanaei, Eslami et al. 2017). Deterministic model has the advantage of being easy to use, but has the disadvantage that it is difficult to reflect indeterminate factors caused by soil and pipe material in underground

pipelines. Therefore, Statistic models such as Markov model(Caleyo, Velázquez et al. 2009, Valor, Caleyo et al. 2013), Monte-Carlo Simulation (MCS) (Ossai, Boswell et al. 2016, Park, Lee et al. 2020) and Time-dependent Generalized Extreme Value Distribution (GEVD) model (Velázquez, van der Weide et al. 2014)may be preferred when applied to a system with high uncertainty due to insufficient corrosion data. Accordingly, several studies have been performed to quantitatively analyze the correlation of the surrounding environmental factors such as pH and water content in the soil to the pipeline reliability. Generally, these works collect data to construct probabilistic models of corrosion depth distribution considering the uncertainty of the parameters that describe the environment characteristics. Generalized extreme value (GEV) distribution is commonly selected to model the defect depth distribution due to the limited number of inspection cases. Previous works have efficiently constructed the probabilistic models by estimating and updating the parameters inferring the distribution(Kale, Thacker et al. 2004, Li, Yu et al. 2009). For instance, Caleyo et al. estimated the parameters of GEV distribution describing corrosion distribution using 60 cases of defects with 80% confidence interval (Caleyo, Velázquez et al.

2009). Researchers analyzed the probability distribution for defect depth using the various corrosion parameters distributions known to follow specific distributions (Melchers 2005, Valor, Rivas et al. 2007, Caleyo, Vela´ zquez et al. 2008, Velázquez, Van Der Weide et al. 2014). The above-mentioned studies focused on obtaining the parameter values to precisely describe the defect depth distribution suitable for the excavation sites or the inspected site where the data is collected, thus the constructed models are inapplicable to general use (Kapusta, Pots et al. 2004, Timashev and Bushinskaya 2010). As the environmental conditions vary region to region, the expensive data acquisition should be repeated whenever a maintenance plan is made. In addition, maintenance of pipeline should be established as a long-term plan and the excavation inspection rarely happens due to the lifetime of pipeline and the slow corrosion process, thus the environmental conditions can be changed in the meantime (Sahraoui, Khelif et al. 2013, Zhang and Zhou 2014, Parvizsedghy, Senouci et al. 2015). Therefore, a generic probabilistic model of defect depth distribution of which parameters can be updated using newly obtained data (Breton, Sanchez-Gheno et al. 2010).

In this study, a framework for efficient estimation of the corrosion depth distribution is suggested to allow the constructed model adapting the changing environmental conditions. The time-dependent GEV distribution model for corrosion growth rate was employed to estimate the depth distribution in a sense that the depth distribution of the target year is calculated by summation of the growth rates and the depths in the previous year. The use of the growth rate model enables the obtained corrosion depth distribution to flexibly reflect the changing environmental conditions. According to the analysis result of the data from the literatures, the parameters of growth rate GEV distribution were assumed to depends on those of the defect depth distribution in the form of exponential function. The parameters of the defect depth growth model are sequentially updated whenever new set of data is available via Bayesian inference with the prior depth distribution which was the posterior distribution at the previous estimation step. In the presented Bayesian framework, since the information of the previous data affects the consecutive estimation of the parameters as the prior distribution, estimation of the parameters for the probabilistic model can be sensitive to the newly obtained data in tandem with being guided by

the previously collected data. Markov chain Monte Carlo (MCMC) was adopted to sample the posterior distribution of the corrosion depth(Wang, Yajima et al. 2015, Ossai, Boswell et al. 2016). The developed corrosion depth model is verified with an accurate model constructed using actual inspection data.

3.2. Adaptive estimation of corrosion defect depth

3.2.1. Time-dependent GEV distribution for corrosion defect depth distribution

GEV distribution is known to be suitable for empirical description of the growth rates of the observed external corrosion defects depth. The probability distribution function (pdf), *f*, of GEV distribution can be expressed as:

$$f(d|\theta) = \begin{cases} \frac{1}{\sigma}\exp\left[-\left\{1+\zeta\left(\frac{d-\mu}{\sigma}\right)\right\}^{-1/\zeta}\right]\left\{1+\zeta\left(\frac{d-\mu}{\sigma}\right)\right\}^{-1-1/\zeta}, & \text{when } \zeta \neq 0 \\ \frac{1}{\sigma}\exp\left\{-\left(\frac{d-\mu}{\sigma}\right)-\exp\left(-\frac{d-\mu}{\sigma}\right)\right\}, & \text{when } \zeta = 0 \end{cases} \quad \text{Eq. (1)}$$

where *d* is the corrosion defect depth (or growth rate in case of rate GEV distribution) and $\theta = (\mu,\ \sigma,\ \zeta)$ is the parameter vector of the GEV distribution. The parameters, $\mu,\ \sigma,$ and ζ, imply the location, scale, shape of the defect growth rate distribution pdf (Caleyo, Valor et al. 2015). The

changes in the corrosion depth growth rate depending on time can be categorized as several groups, and in general, the growth rate is relatively fast at the initial stage of corrosion (Gu, Kania et al. 2002). Since the protective oxide film is formed on the corrosion site over time, the growth rate dwindles. Thus, the distribution of the growth rate changes depending on time, and accordingly, the time-dependent corrosion growth rate models have been employed in the previous studies. Since the parameters of the GEV distribution can be interpreted as the summary of the corrosion depth distribution, the time-dependent GEV adopts its parameters as the functions of time to describe the dependency of corrosion growth rate on time. Here, we assume that each of GEV parameter can be expressed in an exponential function of time, of which required number of parameters is two, referring to the analysis result using inspection data of excavated underground pipelines.

$$(\mu_r(t),\ \sigma_r(t),\ \zeta_r(t)) = (a_\mu \times \mu_d(t)^{b_\mu},\ a_\sigma \times \sigma_d(t)^{b_\sigma},\ a_\zeta \times \zeta_d(t)^{b_\zeta}) \quad \text{Eq. (2)}$$

where a and b indicate the coefficients for corrosion growth rate parameters and the subscripts of the coefficients, μ, σ, and ζ mean which

parameter the coefficients are indicating. In the remaining part, φ, θ_r, and θ_d will indicate the coefficient vector, $(a_\mu,\ b_\mu,\ a_\sigma,\ b_\sigma,\ a_\zeta,\ b_\zeta)$, the defect growth distribution parameter vector, $(\mu_r, \sigma_r, \zeta_r)$, and the defect depth distribution parameter vector, $(\mu_d, \sigma_d, \zeta_d)$. The corrosion depth of t^{th} year, $d(t)$, is calculated by adding the growth rate in the unit of mm/year to the depth of the previous year.

$$d(t) = r(t) + d(t-1), \quad t \geq 1 \qquad \text{Eq. (3)}$$

where $d(0)$ is the initial value of the corrosion depth and assumed to be sampled from a GEV distribution with parameters, $(\mu, \sigma, \zeta) = (0.15, 0.3, 0.015)$, which generates narrow distribution of small corrosion depths. The use of the time-dependent growth rate GEV pdf in Eq. (1) and (2) allows the model of flexibly adapting to the changes in environmental condition by updating only the six coefficients rather than estimating the three parameters whenever a new set of data is available. In tandem with the above-describe model, the generality of the suggested approach can be attained by using of method to update the coefficient.

3.2.2. Adaptive estimation framework using Bayesian inference

The parameters estimation via Bayesian inference can be considered as maximization of the posterior probability that is proportional to likelihood and prior distribution as presented in Eq. (4) (Wang, Yajima et al. 2015). Note that all the values such as probabilities, parameters, and coefficients can vary depending on the time when the data observed, thus for better readability, *t* indicates the time passing from which the pipelines are buried underground and τ indicates the time when the inspection is carried out and the corresponding data is obtained. When $\boldsymbol{D}^{\boldsymbol{\tau}}$ represents the observed corrosion depth data in $t = \tau$ year, then the posterior distribution of the parameter, θ_d, is written as:

$$P^{\tau}(\theta_d|\boldsymbol{D}^{\tau}) \propto \mathcal{L}(\boldsymbol{D}^{\tau}|\theta_d) \times \pi^{\tau}(\theta_d) \quad \text{Eq. (4)}$$

where $\mathcal{L}(\boldsymbol{D}^{\tau}|\theta_d)$ and $\pi^{\tau}(\theta_d)$ indicate the likelihood and prior distribution of θ obtained in τ year. As explained in Section 2.1, θ_d depends on the coefficients, $\varphi = (a_\mu, b_\mu, a_\sigma, b_\sigma, a_\zeta, b_\zeta)$, thus the relation in Eq. (4) should be changed as:

$$P^{\tau}(\varphi|\boldsymbol{D}^{\tau}, \theta_d) \propto \mathcal{L}(\boldsymbol{D}^{\tau}, \theta_d|\varphi) \times \pi^{\tau}(\varphi) \quad \text{Eq. (5)}$$

The prior distributions are fitted to the Gaussian distribution centered at the estimated coefficients. The initial values for the mean and the variance of $\pi^1(\varphi)$ are assumed for the corresponding distribution to have broad range of values referring to the literatures. As the growth rate can not be observed directly, the depth distribution at τ should be calculated using Eq. (2) and (3), repeatedly. The likelihood in Eq. (5) can be calculated by the product of the GEV pdf, $f(d_i^\tau, \theta_d|\varphi)$, in which $d_i^\tau \in \boldsymbol{D}^\tau$.

$$\mathcal{L}(\boldsymbol{D}^\tau, \theta_d|\varphi) = \prod_{d_i^t \in \boldsymbol{D}^t} f(d_i^\tau, \theta_d|\varphi) \quad \text{Eq. (6)}$$

When the defect depths are observed by indirect inspection such as ILI, the measurement errors are unavoidably added to the inspection data. The measurement errors (ME) are reported as additive and having constant value irrelevant to the defect depth. In general, MEs are known to follow normal distribution of which mean is zero and variance is constant. When the pdf representing the probability of the value that the defect of μ depth is actually observed is expressed as $f_{ME}(\mu, \sigma^2) = N(\mu, \sigma^2)$, then the pdf of the observed defect depth under measurement error, $f_{D,ME}(d, \theta_d|\varphi)$ can be derived by a convolutional integral.

$$f_{D,\,ME}(d, \theta_d|\varphi) = \int_0^{\infty} f_D(d, \theta_d|\varphi) \cdot f_{ME}(d - y,\ \sigma'^2) dy \qquad \text{Eq. (7)}$$

where *N* indicates normal distribution. The posterior probability and the likelihood in Eq. (5) and (6) should be transformed as:

$$P^{\tau}(\varphi|\boldsymbol{D}^{\tau},\ \theta_d(\tau)) \ \propto\ \mathcal{L}_{ME}(\boldsymbol{D}^{\tau}, \theta_d(\tau)|\varphi) \times \pi^{\tau}(\varphi)$$
$$\mathcal{L}_{ME}(\boldsymbol{D}^{\tau}, \theta_d|\varphi) = \prod_{d_i \in \boldsymbol{D}^{\tau}} f_{D,\,ME}(d_i, \theta_d|\varphi)$$

where $\mathcal{L}_{ME}(\boldsymbol{D}^{\tau}, \theta_d|\varphi)$ indicates the likelihood considering measurement errors. MCMC with Metropolis-Hastings method is adopted to sample the coefficient posterior distribution (Hazra, Pandey et al. 2020). The posterior distribution obtained in τ year is employed as the prior distribution for estimation of the coefficients in $\tau + \Delta\tau$ year.

$$\pi^{\tau+\Delta\tau}(\varphi) = P^{\tau}(\varphi|\boldsymbol{D}^{\tau}) \qquad \text{Eq. (8)}$$

where τ is the year of data acquisition by excavating pipelines or inspection using ILI and $\Delta\tau$ is the acquisition period. The data obtained up

to τ year do not directly used in estimating the coefficients in $\tau + \Delta\tau$ year, rather the information of the data dissolved in the pdf of the prior distribution guides the procedure of maximum a posteriori (Figure 1). The suggested method is general in a sense that, since the data except for the newly obtained set only indirectly affects, the estimation of the coefficients is relatively sensitive to the trend changes in the data. In addition, when the posterior distribution obtained using the data observed in a specific site is introduced to other site, it serves as an accumulated knowledge to estimate the coefficients for the other site resulting in obtaining accurate estimates with fewer number of observations. The overall procedure to adaptively estimate the distribution parameters is summarized in Figure 3.1.

Step 1. Sample d(0) from the initial depth distribution.
- Initial depth distribution: GEV with $(\mu, \sigma, \zeta) = (0.15, 0.3, 0.015)$,

Step 2. Collect inspection depth data, $\boldsymbol{D}^{\tau}$, at $t = \tau$

Step 3. Samples $\varphi = \{a_\mu, b_\mu, a_\sigma, b_\sigma, a_\zeta, b_\zeta\}$ via MCMC

while collecting N_{mc} number of φ samples required for MCMC analysis

Step 3.1. **while** t <= τ

3.1.1. Calculate GEV parameters for defect growth rate distribution

$$(\mu_r(t),\ \sigma_r(t),\ \zeta_r(t)) = (a_\mu \times \mu_d(t)^{b_\mu},\ a_\sigma \times \sigma_d(t)^{b_\sigma},\ a_\zeta \times \zeta_d(t)^{b_\zeta})$$

3.1.2. Sample from $r(t)$ distribution using GEV with $\left(\mu_r(t), \sigma_r(t), \zeta_r(t)\right)$

3.1.3. Derive $d(t)$ distribution using the relation $d(t) = r(t) + d(t\text{-}1)$

end

Step 3.2. Calculate a posteriori.

- $P^{\tau}(\varphi|\boldsymbol{D}^{\tau}, \theta_d(\tau)) \propto \mathcal{L}_{ME}(\boldsymbol{D}^{\tau}, \theta_d(\tau)|\varphi) \times \pi^{\tau}(\varphi)$

where $f_{D,ME}(d, \theta_d|\varphi) = \int_0^{\infty} f_D(d, \theta_d|\varphi) \cdot f_{ME}(d - y, \sigma'^2)\mathrm{d}y$

$\mathcal{L}_{ME}(\boldsymbol{D}^{\tau}, \theta_d|\varphi) = \prod_{d_i \in \boldsymbol{D}^{\tau}} f_{D,ME}(d_i, \theta_d|\varphi)$

$f_{ME}(\mu, \sigma^2) = N(\mu, \sigma^2)$

Step 3.3. t = t + 1

end

Step 4. Select the most probable φ from the pool of MCMC samples (P_*^{τ})

Step 5. Update φ and the prior distribution

- $\pi^{\tau+\Delta\tau}(\varphi) = P_*^{\tau}$

Step 6. Repeat the above procedure every $\Delta\tau$ period

Figure 3.1. Pseudo code for adaptive estimation of corrosion depth distribution via Bayesian approach

3.3. Implementation

The estimation framework was implemented to three different cases for verification. In each case, we prepared hidden pdf of the corrosion depth distribution and sampled several depths from the hidden distribution. The suggested estimation method is tested if it can identify the hidden corrosion depth distribution. The hidden depth distributions used in each case are extracted from the literature, which constructed the probability model of corrosion depth based on the actual defect depth observation data(Wang, Yajima et al. 2015). The assumptions applied to each of the hidden corrosion depth distribution and the characteristics of each case are summarized in Table 3.1.

Case 1. Data acquired from direct inspection is available.

The first case presents the situation that users of the suggest method can excavate and directly inspect the underground pipelines. In contrast to the indirect inspection, measurement errors are negligible. The defects on the dug pipelines were assumed to be repaired immediately in this case. Considering huge cost of underground pipeline excavation, the maintenance (inspection) term is set to 10 years.

Case 2. Data acquired from indirect inspection is available.

In general, direct excavation of underground pipelines is an unusual occurrence. Indirect inspection such as ILI is a common choice for pipeline maintenance, but the measurement errors are inevitable. The measurement error is assumed to be additive and follow the Gaussian distribution with zero mean and 0.67 mm standard deviation, which is known measurement error of ILI inspection according to the work of Gu et al. The observed defects remain unfixed on the pipeline surface and the inspection period is set to 10 years.

Case 3. Data acquired from indirect inspection is available and parameters of corrosion defect distribution changes over time.

To test the flexibility of the suggested estimation framework, the parameters of the hidden corrosion depth distribution were assumed to undergo a sudden change in the corrosion process. Data observation and the coefficient update occurred six times, and the data obtained at fourth observation was sampled from the distribution with changed

parameters. Except for the change in parameters, the assumptions for the case 3 are the same as the case 2.

Table 3.1. Tested verification cases of corrosion depth estimation

Case	Target situation	Repair	Inspection period ($\Delta\tau$)	Measurement error
1	Direct inspection	Yes & No	10 years	None
2	Indirect inspection	No	10 year	$\varepsilon \sim N(0, 0.67^2 \mathrm{mm}^2)$
3	Indirect inspection	No	10 year	$\varepsilon \sim N(0, 0.67^2 \mathrm{mm}^2)$

3.4. Visualization and discussion

3.4.1. Case 1 – Direct inspection

Figure 3.2 shows the results of the parameter estimation while repairing the observed defect are fixed immediately. The adaptation process indicating the update of the coefficient, φ, at every inspection time period, $\Delta\tau$, seems already finished at the first 10 year because no changes of the estimated distribution can be observed at the time over 10 year. This indicates that the suggested Bayesian framework can construct the predictive distribution model with high accuracy in spite of the small number of available defect data. One problem that can be raised from the results is that, because only six defect depths is available at each τ, the observation data is sometimes not evenly distributed and biased at the lower depth values. That is, the observed data is not capable of reflecting the actual defect depth probability distribution, thus the resulted predictive distribution underestimates the probability of observing higher depth value than what the depth value actually is. This can lead to establishing wrong maintenance plans, which in turn leads to an occurrence of catastrophic event.

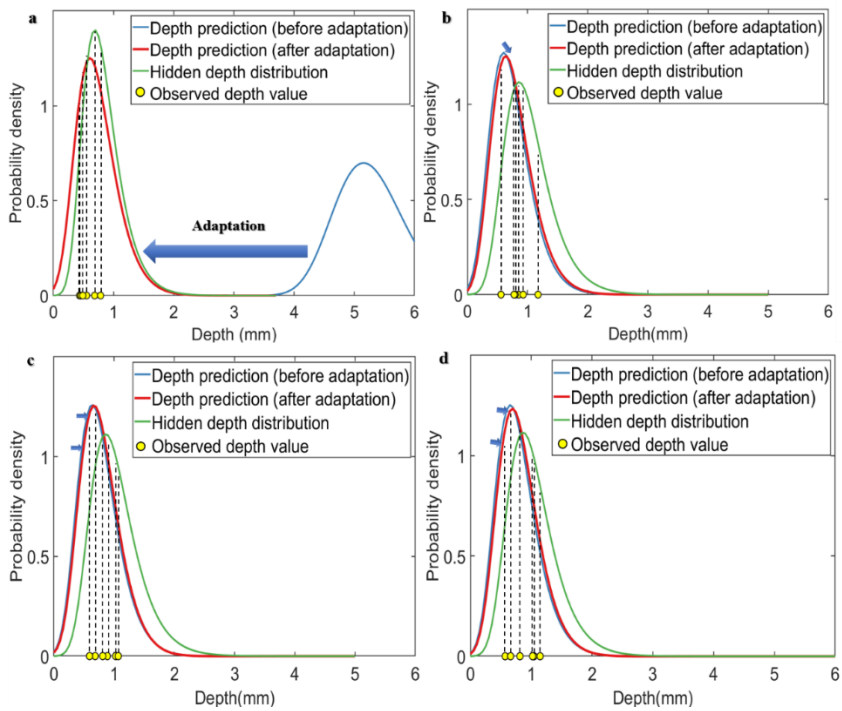

Figure 3.2. Corrosion depth distribution results for Case 1: direct inspection and coefficient estimation using 6 observed defects. a) Estimation at τ=10 year, b) τ=20 year, c) τ=30 year, and d) τ=40 year.

Safety analysis should be conservative and it is better to overly estimate the risks, rather than overlooking them. In this study, an artificial defect depth value, which assumption of normal distribution, is used for estimation of the coefficients. When the number of observed depths is small, the added depth allows the predictive distribution of being conservative. If the acquired available data is abundant, the impact of the artificial depth diminishes and accuracy of the predictive distribution improves obtained by calculating 99 percentile of the observed depth values under the Figure 3.3 shows the corrosion depth distribution results when the available data acquired by indirect inspection and thus the data includes measurement error. In contrast to the Case 1, the defects formed on pipeline were not removed in this case. At the first attempt to estimate the depth distribution (τ =10 year), the depth distribution is largely adjusted to have smaller depth values compared to the distribution before estimation.

3.4.2. Case 2 – indirect inspection

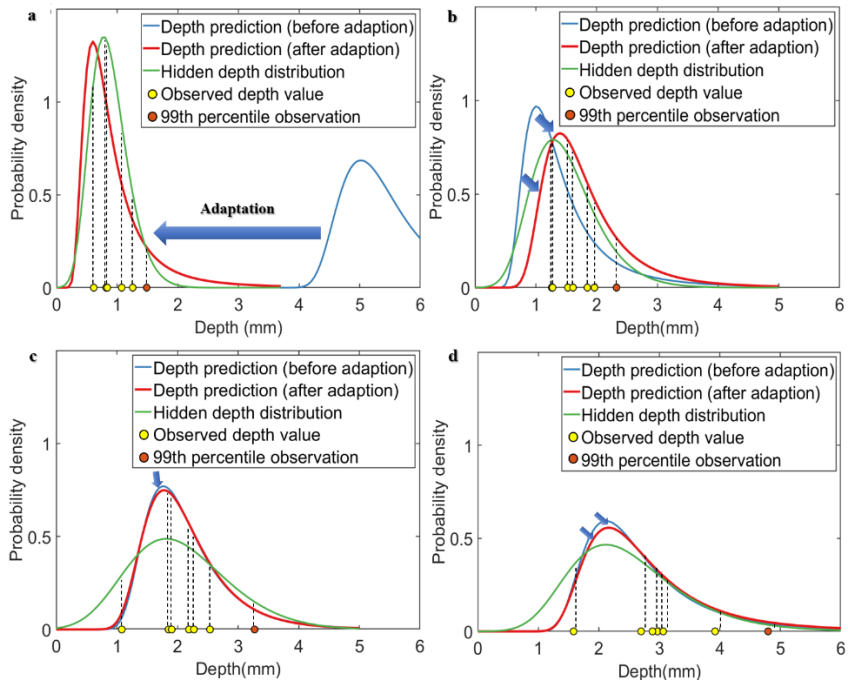

Figure 3.3. Corrosion depth distribution results for Case 2: indirect inspection and coefficient estimation using 6 observed defects. a) Estimation at τ=10 year, b) τ=20 year, c) τ=30 year, and d) τ=40 year.

This is because the initial coefficients, φ, are set to excessively large values, and they were corrected by the first estimation. From the results of Figure 3.3b to 3.3d, the predictive distributions stay still from the previous distribution, indicating that the relation between the depth and growth rate distributions in Eq. (3) is settled down after the first estimation, and can predict the future depth distributions that change depending on the pipeline operation time. This can be checked in Figure 3.4 which shows the posterior distribution of the coefficient estimation. The φ values are fixed at the point obtained in the first estimation, and as the estimation is repeated at every $\Delta\tau$, the uncertainty of the coefficient is gradually reduced. In the posterior distribution of φ estimates in Figure 3.4, φ is widely distributed at $\tau = 10$, indicating that not enough reliability is secured due to the small number of observation data used for estimation. In addition, the variance of the initial prior distribution is set to excessively large value, thus the obtained φ estimates cannot help being distributed widely

over the coefficient ranges. This can be addressed using the narrowly distributed priors obtained from previous studies or field experts. In Figure 3.4, the exponent coefficient, b_μ, is estimated as a negative value indicating that the parameter, μ_r, which represents the location of the defect growth rate GEV distribution is inversely related with the parameter for the location of the defect depth distribution, μ_d. This result is consistent with the previous study reporting that the size of defect depth and the growth rate are inversely correlated, and thus the growth rate decreases as the pipeline operation time passes. The other exponent coefficients, b_σ and b_ζ are shown to be negative as well in Figure 3.4. The negative values of b_σ and b_ζ indicate that the defect growth rate have a tendency of converging at average value over time, and since the mean value of the growth rate decreases owing to the low b_μ, the overall progress of corrosion slows down over time. .

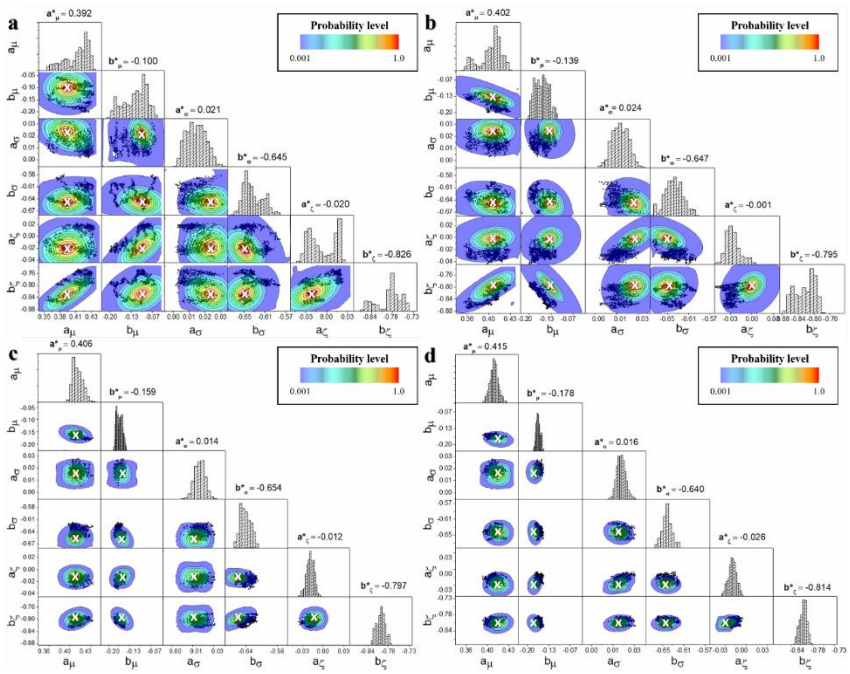

Figure 3.4. Posterior distribution of coefficient estimation for Case 2. a) Estimation at τ=10 year, b) τ=20 year, c) τ=30 year, and d) τ=40 year. The coefficient values with * indicate the mean value of each distribution and the x marks indicate the locations of the mean.

In every results of the constructed predictive distribution in Figure 3.3, the estimated distribution measures the probability of detecting large depth slightly higher than the hidden distribution. This is due to the addition of the artificial data point. In overall, the predictive distribution underestimates the probability of observing small defect depths compared with the hidden depth probability distribution because the inspection data is absent in the lower depth values. The accuracy of the probability distribution in the area of observing lower depth values can be improved by introducing an artificial data point of which the depth value is small, but this may drag down the distribution to lower depth values, resulting in low reliability of pipeline maintenance plans.

Since the coefficient, φ, is robustly evaluated at the first estimation, the probability distributions at $\tau = 20, 30,$ and 40 years seem not changed by adaptation, but it can be check that the probability of observing the average depth value slightly decreases. At every attempt

of estimation, the added artificial depth affects the probability distribution, and the coefficient should be mended to fatten the shape of the adapted distribution curve, which allows the defect depth distribution of not ignoring the probability of high depth value.

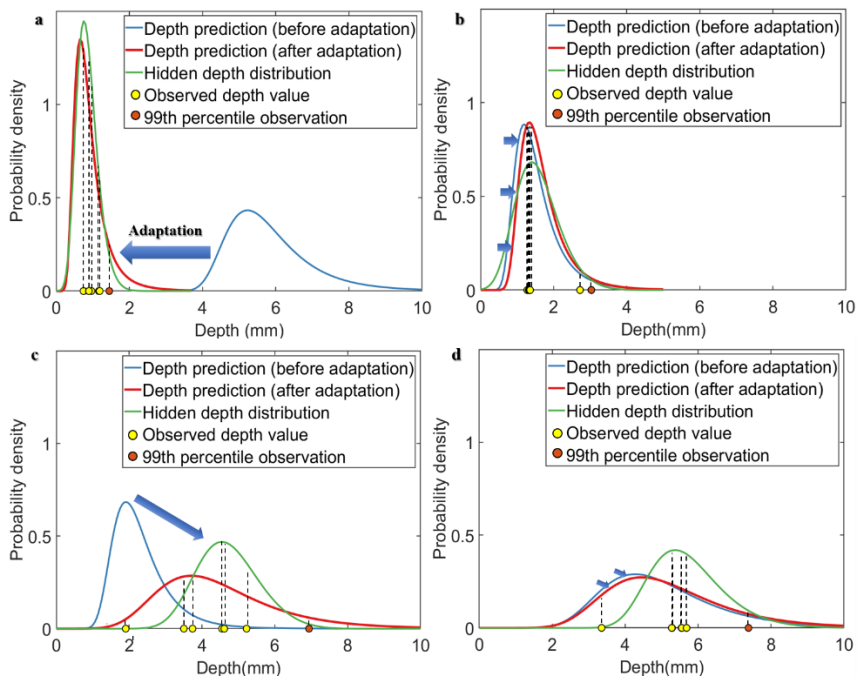

Figure 3.5. Corrosion depth distribution results for Case 3: indirect inspection and coefficient estimation using 6 observed defects. In this case, the environmental condition that surrounds the underground pipelines is suddenly changed between 20 and 30 years of operation. a) Estimation at τ=10 year, b) τ=20 year, c) τ=30 year, and d) τ=40 year.

3.4.3. Case 3 – sudden changes in hidden depth distribution

The suggested framework of predicting the depth distribution does not utilize the past inspection data directly, rather it is reflected as a form of prior distribution. The prior distribution of which probabilities of the coefficients, φ, are updated at every estimation allows the coefficient estimation of flexibly adapting the newly observed data points and robustly predicting the defect depth distribution as it can be seen in Section 3.4.2. Until the second estimation of the coefficients (Figure 3.5a - 3.5b), the estimation results are similar to those of Case 2 in that the predictive distribution overly measures the large defect depths and the only small difference can be found in between the predictive distributions before and after the adaptation. Then, we changed the parameters of the hidden depth distribution to be shifted to larger depth values, and accordingly, the observed data suddenly increases larger than what might be observed by the original hidden distribution in Figure 3.4c. The predictive distribution is adapted

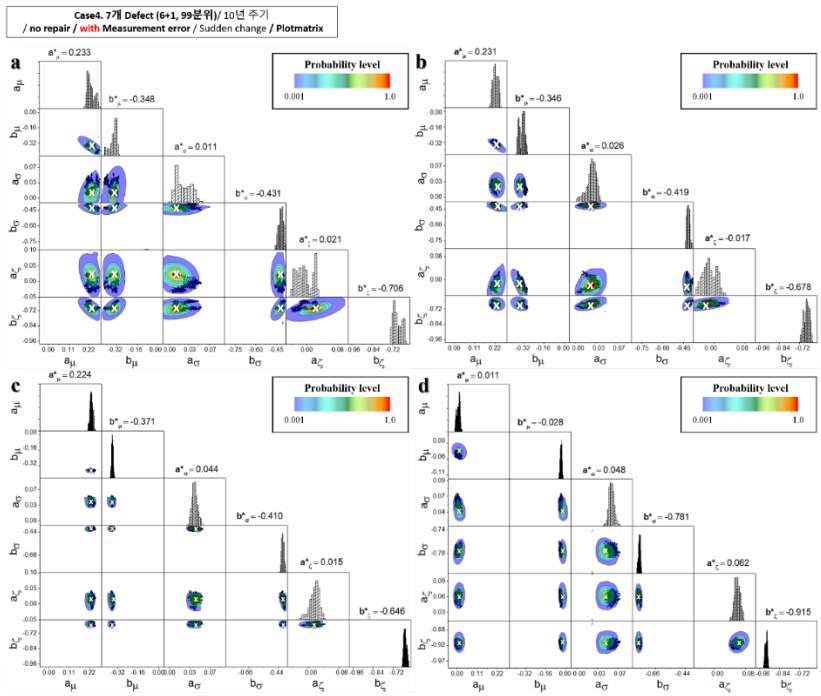

Figure 3.6. Posterior distribution of coefficient estimation for Case 3. a) Estimation at τ=10 year, b) τ=20 year, c) τ=30 year, and d) τ=40 year. The coefficient values with * indicate the mean value of each distribution and the x marks indicate the locations of the mean.

promptly to the change trend of the observed defect depths in Figure 3.4c. However, the predictive distribution after the adaptation distributed widely compared with the hidden distribution, which can be explained by the following two reasons. First of all, it is because the defect depth values used when estimating the coefficients, φ. The smallest defect observed in $\tau = 30$ is placed outside of the hidden depth distribution due to the measurement error, resulting in the predictive distribution distorted to overly estimate the probability of observing small defects. Meanwhile, the artificial data obtained by 99 percentile point of data points affects the predictive distribution, which leads to slightly higher probability in observing large defects by the predictive distribution than the hidden one. This intentional inaccuracy allows us of establishing conservative maintenance plan at the cost of slightly higher safety cost. The second reason for the wide predictive distribution, specifically for the smaller defects is that the prior distributions of the coefficient were updated before the hidden depth

distribution is changed to have tendency of large defect values. Thus, the prior distribution used for MAP estimation at $\tau = 30$ indicated high probability of the φ value that induces the defect depth distribution centered at low values. In this case, the maximum likelihood estimation without prior probability would present more accurate results in predicting the depth values than MAP, but the benefits that can secure from using the prior probability precedes the disadvantage of it because it can guarantee higher reliability of estimation. In Figure 3.6, which shows the posterior distribution of φ in Case 3, the MCMC sampling data points are gathered in narrower area as the pipeline operating time passes. That is, the variance of φ decreases despite of the changed trend in the observation data. In sum, the prior distribution allows the estimation process of rapidly adapting the changing environment using scarce data points with high reliability. In addition, the artificial data point prevents the predicted distribution

from biased to predicting small defects even when the priors of the coefficients indicate the distribution centered at low defect values.

3.5. Conclusion

A framework for efficient estimation of the corrosion depth distribution is suggested to allow the constructed model adapting the changing environmental conditions. In bid to consider the dependency of the corrosion growth rate distribution on time, the parameters of the growth rate distribution are assumed to be correlated to the present depth distribution. The use of the growth rate model enables the obtained corrosion depth distribution to flexibly reflect the changing environmental conditions. The coefficients of the defect depth – growth rate relation are sequentially updated via Bayesian inference with the prior depth distribution which was the posterior distribution at the previous estimation step.

The suggested method to construct predictive distribution models for corrosion defects is verified using the simulated observation data. Although the estimation uses only six data points for all the tested

cases, the estimation method accurately predicts the defect depth distribution. When the observed defects are biased to small values, the added artificial depth data allows conservative construction of the predictive defect depth distribution model by overly evaluates the probability of forming large defects. The adaptive estimation method sensitively moved the predictive defect distribution suitable to changing environment with high reliability by not using the past observation data directly, rather using them in the form on the prior distribution.

CHAPTER 4. Concluding Remarks

In this study, we conducted risk analysis and risk reduction studies for the safe design of hydrogen refueling stations. In addition, the Bayesian-based methodology, which can predict corrosion damage of external hydrogen pipes, allows the prediction model to be modified by taking into account more actual observations.

All three processes in this study for analyzing the risk of hydrogen refueling station: Tube-trailer, NG & LPG steam reforming were found to exceed Tolerable risk levels in areas with some population density under currently known process conditions. Therefore, it is possible to safely design the process by changing the conditions of the process units that most affect the risk little by little and modifying the process to lower the risk.

In conclusion, by installing a firewall, it is possible to design a process with a tolerable risk level by reducing the overall risk by reducing the frequency of accidents.

References

HR Gye. et al. (2019); Benjamin L. et al. (2019); Gasification, E. B. L. (2006); Silva, P. P., et al. (2015); G. Parks, R. Boyd. et al.(2014); Yan-Lei L, et al.(2010); R. Ortiz Cebolla, et al.(2015); A. Perna, et al. (2011)

Benjamin L. et al. (2019); Gasification, E. B. L. (2006); G. Parks, R. Boyd. et al.(2014); Yan-Lei L, et al.(2010); R. Ortiz Cebolla, et al.(2015)

Perna, et al.(2011), Silva, P. P., et al. (2015)

CCPS., 2000; Shariff and Leong, 2009; Medina et al.,2009; Patel et al.,2010; Medina-Herrera et al. ,2014

A.Gabbar, H. and H. A. Kishawy (2011). "Framework of pipeline integrity management." International Journal of Process Systems Engineering **1**.

Adetunji, O. (2013). Modeling and Simulation of Pipeline Corrosion in the Oil and Gas Industries**:** 375-394.

Breton, T., J. Sanchez-Gheno, J. Alamilla and J. J. J. o. h. m. Alvarez-Ramirez (2010). "Identification of failure type in corroded pipelines: A Bayesian probabilistic approach." **179**(1-3): 628-634.

Caleyo, F., A. Valor, L. Alfonso, J. Vidal, E. Perez-Baruch and J. M. Hallen (2015). "Bayesian analysis of external corrosion data of non-piggable underground pipelines." Corrosion Science **90**: 33-45.

Caleyo, F., J. Vela´ zquez, J. Hallen, J. Araujo and E. Perez-Baruch (2008). On the probabilistic distribution of external pitting corrosion rate in buried pipelines. International Pipeline Conference.

Caleyo, F., J. Velázquez, A. Valor and J. Hallen (2009). "Probability distribution of pitting corrosion depth and rate in underground pipelines: A Monte Carlo Study." Corrosion Science **51**: 1925-1934.

Caleyo, F., J. C. Velázquez, A. Valor and J. M. Hallen (2009). "Markov chain modelling of pitting corrosion in underground pipelines." Corrosion Science **51**(9): 2197-2207.

Chen, G. H. and J. J. Wu (2015). "Reliability Analysis and Case Study of Long Term Service Gas Pipelines beneath Urban Street." Procedia Engineering **130**: 1478-1485.

Gomes, W. J. S., A. T. Beck and T. Haukaas (2013). "Optimal inspection planning for onshore pipelines subject to external corrosion." Reliability Engineering & System Safety **118**: 18-27.

Gu, B., R. Kania, S. Sharma and M. Gao (2002). Approach to Assessment of Corrosion Growth in Pipelines. 2002 4th International Pipeline Conference.

Hazra, I., M. D. Pandey and N. Manzana (2020). "Approximate Bayesian computation (ABC) method for estimating parameters of the gamma process using noisy data." Reliability Engineering & System Safety **198**: 106780.

Kale, A., B. H. Thacker, N. Sridhar and C. J. Waldhart (2004). A probabilistic model for internal corrosion of gas pipelines. 2004 International Pipeline Conference, American Society of Mechanical Engineers Digital Collection.

Kapusta, S. D., B. F. Pots and I. J. Rippon (2004). The application of corrosion prediction models to the design and operation of pipelines. CORROSION 2004, Nace International.

Li, S.-X., S.-R. Yu, H.-L. Zeng, J.-H. Li and R. Liang (2009). "Predicting corrosion remaining life of underground pipelines with a mechanically-based probabilistic model." Journal of Petroleum Science and Engineering **65**(3): 162-166.

Melchers, R. E. J. C. (2005). "Statistical Characterization of Pitting Corrosion—Part 2: Probabilistic Modeling for Maximum Pit Depth." **61**(8): 766-777.

Ossai, C. I., B. Boswell and I. J. Davies (2016). "Application of Markov modelling and Monte Carlo simulation technique in failure probability estimation — A consideration of corrosion defects of internally corroded pipelines." Engineering Failure Analysis **68**: 159-171.

Ossai, C. I., B. Boswell and I. J. E. f. a. Davies (2016). "Markov chain modelling for time evolution of internal pitting corrosion distribution of oil and gas pipelines." **60**: 209-228.

Park, K., G. Lee, C. Kim, J. Kim, K. Rhie and W. B. Lee (2020). "Comprehensive framework for underground pipeline management with reliability and cost factors using Monte Carlo simulation." Journal of Loss Prevention in the Process Industries **63**: 104035.

Parvizsedghy, L., A. Senouci, T. Zayed, S. F. Mirahadi, M. S. J. S. El-Abbasy and I. Engineering (2015). "Condition-based maintenance decision support system for oil and gas pipelines." **11**(10): 1323-1337.

Sahraoui, Y., R. Khelif, A. J. I. j. o. p. v. Chateauneuf and piping (2013). "Maintenance planning under imperfect inspections of corroded pipelines." **104**: 76-82.

Timashev, S. and A. Bushinskaya (2010). Practical methodology of predictive maintenance for pipelines. 2010 8th International Pipeline Conference, American Society of Mechanical Engineers Digital Collection.

Valor, A., F. Caleyo, L. Alfonso, J. C. Velázquez and J. M. Hallen (2013). "Markov Chain Models for the Stochastic Modeling of Pitting Corrosion." Mathematical Problems in Engineering **2013**: 108386.

Valor, A., D. Rivas, F. Caleyo and J. J. C. Hallen (2007). "Discussion: statistical characterization of pitting corrosion—Part 1: Data analysis and part 2: Probabilistic modeling for maximum pit depth." **63**(2): 107-113.

Vanaei, H. R., A. Eslami and A. Egbewande (2017). "A review on pipeline corrosion, in-line inspection (ILI), and corrosion growth rate

models." International Journal of Pressure Vessels and Piping **149**: 43-54.

Velázquez, J., H. van der Weide, E. Hernandez-sÁNchez and H. Hernández (2014). "Statistical Modelling of Pitting Corrosion: Extrapolation of the Maximum Pit Depth-Growth." International Journal of Electrochemical Science **9**: 4129-4143.

Velázquez, J., J. Van Der Weide, E. Hernández and H. Herrera Hernández (2014). "Statistical modelling of pitting corrosion: extrapolation of the maximum pit depth-growth."

Wang, H., A. Yajima, R. Y. Liang*, H. J. C. A. C. Castaneda and I. Engineering (2015). "Bayesian modeling of external corrosion in underground pipelines based on the integration of Markov chain Monte Carlo techniques and clustered inspection data." **30**(4): 300-316.

Wang, H., A. Yajima, R. Y. Liang and H. Castaneda (2015). "A Bayesian model framework for calibrating ultrasonic in-line inspection data and estimating actual external corrosion depth in buried pipeline utilizing a clustering technique." Structural Safety **54**: 19-31.

Zhang, S. and W. J. E. S. Zhou (2014). "Cost-based optimal maintenance decisions for corroding natural gas pipelines based on stochastic degradation models." **74**: 74-85.

CSA (2007). Oil and gas pipeline systems. Commentary on CSA Z662-07, Canadian Standard Association.

EGIG (2015). Gas Pipeline Incidents, 9th Report of the European Gas Pipeline Incident Data Group(Period 1970-2013). EGIG 14. R. 0403, EGIG.